THE UNIVERSITY of EDINBURGH

Edinburgh Research Explorer

Teriflunomide treatment for multiple sclerosis modulates T cell mitochondrial respiration with affinity-dependent effects

Citation for published version:
Klotz, L, Eschborn, M, Lindner, M, Liebmann, M, Herold, M, Janoschka, C, Torres Garrido, B, Schulte-Mecklenbeck, A, Gross, CC, Breuer, J, Hundehege, P, Posevitz, V, Pignolet, B, Nebel, G, Glander, S, Freise, N, Austermann, J, Wirth, T, Campbell, GR, Schneider-Hohendorf, T, Eveslage, M, Brassat, D, Schwab, N, Loser, K, Roth, J, Busch, KB, Stoll, M, Mahad, DJ, Meuth, SG, Turner, T, Bar-Or, A & Wiendl, H 2019, 'Teriflunomide treatment for multiple sclerosis modulates T cell mitochondrial respiration with affinity-dependent effects', *Science Translational Medicine*, vol. 11, no. 490, eaao5563. https://doi.org/10.1126/scitranslmed.aao5563

Digital Object Identifier (DOI):
10.1126/scitranslmed.aao5563

Link:
Link to publication record in Edinburgh Research Explorer

Document Version:
Peer reviewed version

Published In:
Science Translational Medicine

Publisher Rights Statement:
This is the authors' peer-reviewed manuscript as accepted for publication.

General rights
Copyright for the publications made accessible via the Edinburgh Research Explorer is retained by the author(s) and / or other copyright owners and it is a condition of accessing these publications that users recognise and abide by the legal requirements associated with these rights.

Take down policy
The University of Edinburgh has made every reasonable effort to ensure that Edinburgh Research Explorer content complies with UK legislation. If you believe that the public display of this file breaches copyright please contact openaccess@ed.ac.uk providing details, and we will remove access to the work immediately and investigate your claim.

Download date: 05. May. 2023

Science Translational Medicine AAAS

Submitted Manuscript: Confidential template updated: February 28 2012

Title: **Therapeutic inhibition of mitochondrial respiration modulates antigen-specific immune responses in an affinity-dependent fashion: implications for the role of teriflunomide in Multiple Sclerosis**

Authors: L. Klotz[1+*], M. Eschborn[1+], M. Lindner[1+], M. Liebmann[1], M. Herold[1], C. Janoschka[1], B. Torres Garrido[1], A. Schulte-Mecklenbeck[1], C.C. Gross[1], J. Breuer[1], P. Hundehege[1], V. Posevitz[1], B. Pignolet[2], G. Nebel[3], S. Glander[4], N. Freise[5], J. Austermann[5], T. Wirth[1], G. R. Campbell[6], T. Schneider-Hohendorf[1], M. Eveslage[7], D. Brassat[8], N. Schwab[1], , K. Loser[9], J. Roth[5], K. B. Busch[3], M. Stoll[4], D. J. Mahad[6], S. G. Meuth[1], T. Turner[10], A. Bar-Or[11], H. Wiendl[1] on behalf of the TERIDYNAMIC study group

Affiliations:

[1]University Hospital Münster, Department of Neurology with Institute of Translational Neurology, Münster, DE

[2]INSERM U1043 - CNRS UMR 5282, Centre de Physiopathologie Toulouse-Purpan, Université Toulouse III, Toulouse, France

[3]University of Münster, Institute of Molecular Cell Biology, Münster, DE

[4]University of Münster, Department of Genetic Epidemiology, Münster, DE

[5]University of Münster, Department of Immunology, Münster, DE

[6]University of Edinburgh, Centre for Clinical Brain Sciences, Edinburgh, UK

[7]University of Münster, Institute of Biostatistics and Clinical Research, Münster, DE

[8]CRC-SEP, Neurosciences Departement, Toulouse Universitary Hospital, Toulouse, France

[9]University Hospital Münster, Department of Dermatology, Münster, DE

[10]Sanofi Genzyme, Cambridge, MA, USA

[11]Center for Neuroinflammation and Experimental Therapeutics and Department of Neurology, Perelman School of Medicine, University of Pennsylvania, Philadelphia, PA, USA

[+]equal contribution

*To whom correspondence should be addressed: Luisa Klotz, Luisa.klotz@ukmuenster.de

Abstract:

Interference with immune cell proliferation represents a successful treatment strategy in T cell-mediated autoimmune diseases such as rheumatoid arthritis and multiple sclerosis (MS). One prominent example is pharmacological inhibition of the mitochondrial enzyme dihydroorotate dehydrogenase (DHODH), which interferes with *de novo* pyrimidine synthesis in actively proliferating T and B lymphocytes. Within the TERIDYNAMIC clinical study we observed that the reversible DHODH inhibitor teriflunomide unexpectedly caused selective changes in T cell subset composition and T cell receptor repertoire diversity in relapsing-remitting MS (RRMS) patients. Using a preclinical antigen-specific setup, we saw that DHODH-inhibition preferentially suppressed the proliferation of high-affinity T cells. Mechanistically, DHODH inhibition interferes with oxidative phosphorylation and aerobic glycolysis in activated T cells via functional inhibition of complex III of the respiratory chain. Interestingly, the affinity-dependent effects of DHODH inhibition were closely linked to differences in T cell metabolism. High-affinity T cells are more dependent on oxidative phosphorylation during early T cell activation, which explains their increased susceptibility towards DHODH inhibition. In a mouse model of CNS autoimmunity, DHODH inhibitory treatment also resulted in preferential inhibition of high-affinity autoreactive T cell clones. Importantly, T cells from RRMS patients exhibited increased levels of oxidative phosphorylation and glycolysis compared to T cells from healthy controls, which were reduced with teriflunomide treatment. Together, these data point to a novel mechanism of action where DHODH inhibition corrects metabolic disturbances in T cells, which primarily affects profoundly metabolically active high-affinity T cell clones. Hence, this may promote recovery of an altered T cell receptor repertoire in MS and other autoimmune diseases.

One Sentence Summary: Inhibition of a mitochondrial enzyme by pharmacological DHODH inhibition modulates antigen-specific immune responses in an affinity-dependent fashion.

Introduction

As documented in several successful clinical trials, inhibition of *de novo* pyrimidine synthesis, which is crucial for rapid expansion of activated lymphocytes, is a well-established strategy for treatment of T cell-mediated autoimmune diseases such as rheumatoid arthritis (RA) and multiple sclerosis (MS) *(1–6)*. Leflunomide, along with its active metabolite teriflunomide, are well known inhibitors of the mitochondrial enzyme dihydroorotate dehydrogenase (DHODH), the fourth enzyme in the *de novo* pyrimidine biosynthetic pathway. Both preclinical data and data sets from clinical trials illustrate the impact of pharmacological DHODH inhibition on lymphocyte proliferation and expansion *(7–9)*. However, as illustrated by a recently published placebo-controlled trial *(10)*, it is still poorly understood how these drugs exert a selective effect on autoreactive T cells while only slightly affecting immune responses against bacteria and viruses. Although antibody titers for *de novo* immune responses were slightly impaired in this study, they were sufficient for seroprotection, while cellular memory responses to recall antigens were not affected. It has been proposed that the inhibitory effect of teriflunomide on lymphocyte proliferation might depend on the antigen used for T cell activation; however, this has not been experimentally addressed so far *(11)*.

It has been demonstrated that development of autoimmunity can be driven by avidity maturation of prevailing autoantigen-specific T cell populations. Selective depletion of high-affinity T cell clones can prevent development of organ-specific autoimmunity, e.g. in an animal model of autoimmune diabetes. Likewise, an increase in antigen-affinities has been implicated in disease progression in different models of T cell-mediated autoimmunity *(12–14)*. Also, in an animal model of MS, transgenic mice bearing a higher affinity autoantigen-specific T cell receptor (TCR) exhibit a significantly higher disease incidence than mice with a low affinity TCR for the same antigen, demonstrating that high-affinity T cells bear high pathogenicity also in central nervous system (CNS) autoimmunity. Based on the SKG mouse model, a model for spontaneous arthritis, it has also been proposed that in RA, high-avidity autoreactive T cells might be central to disease pathogenesis,

although this has not been formally proven *(15)*.

The process of lymphocyte activation, expansion and acquisition of effector functions is unique with regard to the specific bioenergetic as well as biosynthetic needs of these cells. In recent years, several studies have elucidated the metabolic properties and requirements of distinct lymphocyte populations under different conditions. In a nutshell, resting T cells primarily use oxidative phosphorylation (OXPHOS) and the breakdown of fatty acids via the tricarboxylic acid (TCA) cycle to supply energy *(16, 17)*. Upon activation, they rapidly switch to aerobic glycolysis to ensure energy supply as well as generating macromolecules and "building blocks" to enable cell growth and expansion. However, despite these general principles, there are fundamental differences in the metabolic profile of distinct lymphocyte populations depending on their activation state. For example, naïve T cells depend on the combined upregulation of OXPHOS and aerobic glycolysis for initiation of T cell proliferation, whereas effector T cells mainly depend on glycolysis for fulfillment of effector functions *(18)*. Moreover, activated memory T cells display an increased capacity for OXPHOS in comparison to freshly activated T cells, which is the basis for their bioenergetic advantage over naïve T cells and explains their increased expansion kinetics *(19)*. These insights into the distinct bioenergetic profiles of T cells gave rise to the concept of immune-metabolism as a novel therapeutic target, allowing a more selective interference with distinct immune cell subsets or activation states.

Here, we demonstrate that teriflunomide treatment of relapsing-remitting MS (RRMS) patients resulted in a reduction in TCR repertoire diversity due to depletion of individual T cell clones (results from an "in depth" immune profiling controlled clinical study in RRMS patients and healthy controls (HCs), TERIDYNAMIC). Following this line, we observed that the extent of teriflunomide-mediated inhibitory effects on T cell proliferation depended on the antigen-affinity of T cells, as high-affinity T cells were much more affected by teriflunomide compared to low-affinity T cells. Interestingly, DHODH inhibition resulted in a profound decrease in OXPHOS as well as aerobic glycolysis of activated T cells, thus directly linking DHODH with the immune-metabolism of T cells. During initial T cell activation, OXPHOS inhibition seemed to be especially

pivotal for DHODH-mediated interference with T cell proliferation. Accordingly, the differential response of high-affinity and low-affinity T cells can be explained by different metabolic demands depending on their antigen-affinity, as high-affinity T cells exhibited a greater dependence on OXPHOS than low-affinity T cells. Hence, our study demonstrates that DHODH inhibition exerts specific effects on distinct T cell clones based on their individual metabolic profiles, thus providing novel insights into the mechanisms underlying the selective immune interference in the context of autoimmune diseases while preserving protective immunity against pathogens.

Results

DHODH inhibition causes distinct alterations in T cell subsets and the T cell receptor repertoire of patients with RRMS

So far, the *in vivo* effects of teriflunomide on T cell subsets in RRMS patients have not been fully elucidated. To address this question, we investigated the $CD4^+$ T cell subset composition in RRMS patients before and during teriflunomide treatment by multi-color flow cytometry as part of the TERIDYNAMIC clinical trial (NCT01863888). Baseline data from 50 RRMS patients are depicted in Table S1. As the known antiproliferative effects of teriflunomide treatment include a mild but consistent lymphopenia *(1)* (Table 1), we assumed that teriflunomide treatment would result in a uniform reduction in T cell subset counts in the peripheral blood of RRMS patients. Surprisingly, we observed distinct effects of teriflunomide treatment on different T cell subsets with an absolute reduction in T helper 1 (Th1) cells, but not Th2 or Th17 cells (Fig. 1 A). While absolute numbers of regulatory T cells (Treg) and of the subset of inducible regulatory T cells (iTregs) remained unaffected (Fig. 1 A, Fig. S1, A and B), we observed a selective increase in the proportion of inducible regulatory T cells (iTreg) under teriflunomide (Fig. 1 B; Fig. S1, A and B). This relative increase in iTregs was even more pronounced in a subgroup of previously untreated RRMS patients receiving teriflunomide (Fig. S1, C and D). Accordingly, this differential effect of teriflunomide resulted in an increased ratio of iTregs/Th1, whereas the ratio of iTregs/Th17 was not modified (Fig. S1 E). With regard to markers of

Treg functionality, expression levels of CD39 and CTLA-4 remained unchanged under teriflunomide treatment (Fig. S1, F and G). In this line, the suppressive capacity of Tregs derived from teriflunomide-treated RRMS patients in an autologous suppression assay was not significantly altered when compared to their respective baseline levels (Fig. S1 H). Likewise, the cytokine profile of Tregs from teriflunomide-treated patients was unaffected (Fig. S1 I).

Based on these results we hypothesized that such differential effects on distinct T cell populations might in turn result in changes of the TCR repertoire, as some T cell clones might be more affected than others. First, we performed a detailed analysis of the TCR repertoire from 14 treatment-naïve RRMS patients at an early disease stage in comparison with 10 age-and sex-matched HCs. Here we observed significant differences in the TCR repertoire between treatment-naïve RRMS patients and HCs (Fig. 1, C and D) characterized by an increase in TCR repertoire diversity reflected by higher numbers of unique clones in the $CD4^+$ compartment and - to a lesser extent in the $CD8^+$ compartment. Moreover, patients with RRMS exhibited a greater percentage of clones with shared amino acid sequences (termed sample overlap), which indicates that the frequency of common or shared clones is higher in RRMS patients than in HCs (Fig. 1, C and D). Importantly, teriflunomide treatment in the TERIDYNAMIC clinical trial resulted in a reduction in $CD4^+$ TCR repertoire diversity within several weeks after treatment initiation, as numbers of unique clones were significantly reduced upon treatment (Fig. 1 E). Additionally, teriflunomide treatment resulted in a significant decrease in sample overlap in RRMS patients, suggesting a reduction of shared clones by teriflunomide (Fig. 1 E). For $CD8^+$ T cells similar, albeit less pronounced teriflunomide-induced changes were observed (Fig. 1 F). To exclude potential confounding effects of previous disease modifying treatments (DMT) on the TCR repertoire, we performed a second analysis focusing on treatment-naïve RRMS patients before and during teriflunomide treatment and could corroborate the effects of teriflunomide on the TCR repertoire (Fig. S1, J and K). Importantly, we did not observe alterations in $CD4^+$ TCR repertoire diversity in RRMS patients following immune-modulatory treatment with dimethyl fumarate (DMF), interferon-β (IFNβ) or glatiramer acetate (GLAT) (Fig. 1, G and H). These results indicate that immune modulation *per se* does not result in TCR repertoire changes *(20)*.

These differential effects suggest that some T cells might be more susceptible towards DHODH-mediated changes than others, which implies the presence of a preferential effect of DHODH inhibition on distinct T cell clones. In order to investigate the DHODH-mediated impact on antigen-specific T cell responses in more detail, we switched to the murine system employing T cells from transgenic mice that are specific for distinct model antigens.

Affinity-dependent effects of DHODH inhibition on T cell proliferation

We compared the effects of DHODH inhibition on T cell proliferation by employing transgenic T cells that recognize antigenic peptides with different antigen-affinities. First, to evaluate the effect of teriflunomide on $CD4^+$ T cells we made use of myelin oligodendrocyte glycoprotein (MOG)-specific T cells from 2D2 mice, which are known to cross-react with a particular neurofilament (NFM_{15-35}) peptide *(21)* with a higher affinity than their cognate MOG_{35-55} peptide as shown by Rosenthal *et al. (22)*. Interestingly, we could demonstrate that teriflunomide was more effective in restricting proliferation of $CD4^+$ T cells upon high-affinity stimulation compared to low-affinity stimulation (Fig. 2, A and B). This was accompanied by a differential effect on $CD4^+$ T cell expansion with a 91 % inhibition of high-affinity stimulated $CD4^+$ T cells compared to 59 % inhibition of low-affinity stimulated $CD4^+$ T cells (Fig. 2 C), while the viability of cells was not affected (Fig. S2 A).

For further corroboration we switched to transgenic $CD8^+$ T cells from OT-I mice recognizing altered peptide ligands of the model antigen ovalbumin with distinct antigen-affinities (SIINFEKL>SIIQFEKL>SIITFEKL) (Fig. 2, D-F) *(23)*. Again, we observed a differential effect of DHODH inhibition depending on the affinity of the peptide used, which was furthermore illustrated by generation analysis of proliferating $CD8^+$ T cells (Fig. 2 D). Importantly, this differential effect cannot be explained by mere quantitative differences in T cell activation, as it was observed among different antigen concentrations (Fig. S2 B).

Finally, we made use of transgenic T cells recognizing an identical peptide albeit with distinct antigen-affinities. Therefore, we employed OT-I transgenic T cells recognizing the ovalbumin peptide SIINFEKL with a high affinity and transgenic T cells from OT-III that are specific for the same antigen, but with a lower affinity *(24)*.

Again, teriflunomide was much more effective in restricting proliferation of high-affinity $CD8^+$ T cells compared to low-affinity $CD8^+$ T cells (Fig. 2, G-I). Importantly, polyclonal stimulation of high- versus low-affinity $CD8^+$ T cells abrogated teriflunomide-mediated differences in T cell proliferation (Fig. S2, C and D), illustrating that the observed differences are indeed linked to antigen-specific stimulation.

In contrast to the strong anti-proliferative effect we did not observe a significant effect of DHODH inhibition on effector molecule production when evaluating IFNγ as well as granzyme B production by both high-affinity and low-affinity $CD4^+$ and $CD8^+$ T cells on a *per cell* basis using intracellular flow cytometry (Fig. S2, E-H). Hence, the well-known *(25, 26)* and robust decrease in proinflammatory cytokine secretion in the supernatants of teriflunomide-treated T cells is thus most likely due to inhibition of T cell expansion rather than a direct effect on cytokine production on a cellular level (Fig. S2, I and J).

Further experiments revealed that a structurally distinct DHODH inhibitor, brequinar, exerted comparable affinity-dependent effects on T cell proliferation (Fig. S3, A-C). Importantly, other anti-proliferative drugs such as the purine synthesis inhibitor mercaptopurine and the DNA intercalating agent mitoxantrone did not exhibit any affinity-dependent effects over a range of concentrations despite robust interference with T cell proliferation (Fig. S3, A-D). Following this line, we observed that the affinity-dependent effects of teriflunomide and brequinar on T cell proliferation could be rescued upon addition of the pyrimidine base uridine, but not the purine base guanosine (Fig. S3 E), further illustrating that inhibition of DHODH-mediated *de novo* pyrimidine synthesis is indeed pivotal for teriflunomide-mediated effects on T cell proliferation; therefore, these data do not support a profound DHODH-independent effect of teriflunomide.

DHODH inhibition interferes with energy generation via OXPHOS and aerobic glycolysis

In light of the intimate topological relationship of DHODH with components of the electron transport chain we wondered whether pharmacological DHODH inhibition might affect oxidative phosphorylation (OXPHOS) in activated T cells. Indeed, in the presence of teriflunomide, OXPHOS was significantly impaired in activated

$CD4^+$ as well as $CD8^+$ T cells (Fig. 3, A-D). In naïve T cells, where generally low OXPHOS activity is observed, this effect could not be seen (Fig. 3, B and D; Fig S4, A and B). Also brequinar, a structurally distinct DHODH inhibitor, reduced the ability for maximal respiration (Fig. S4 C). In accordance with the role of DHODH, uridine supplementation was capable to rescue impaired OXPHOS by teriflunomide (Fig. S4 D). Interestingly, aerobic glycolysis was also severely impaired in activated $CD4^+$ and $CD8^+$ T cells in the presence of teriflunomide (Fig. 3, E-H; Fig. S4, E and F). Importantly, detailed kinetic analysis revealed that teriflunomide-mediated inhibition of $CD8^+$ T cell proliferation was only effective during the first 24h of T cell activation, whereas DHODH inhibition at later time points only marginally affected T cell proliferation (Fig. 3 I). The inhibitory effect of teriflunomide on mitochondrial respiration itself was independent from the time point of initiation during T cell activation, as it was equally suppressed upon initiation at different time points throughout the 48h of T cell activation (Fig. 3 J). The same was observed with respect to aerobic glycolysis (Fig. 3 J). Thus, it can be concluded that OXPHOS is required during the initial phase of T cell proliferation, i.e. during the first 24h, whereas at later time points, DHODH-mediated inhibition of OXPHOS does not critically influence T cell proliferation. Following this line, we analyzed T cell proliferation in the presence or absence of low doses of oligomycin, an ATP synthase inhibitor, at different time points. As expected, initiation of proliferation was substantially impaired in the presence of even low doses of oligomycin (5-10 nM) (Fig. S4 G), again demonstrating that the initiation of proliferation requires mitochondrial ATP synthesis (Fig. S4 H). In contrast, oligomycin did not influence proliferation of already actively proliferating T cells and hence did not abolish the DHODH-mediated inhibitory effects on T cell proliferation (Fig. S4, I and J). These data corroborate our hypothesis that DHODH-mediated OXPHOS inhibition is critical during the early stages of T cell proliferation but dispensable later on. Finally, we addressed whether selective interference with OXPHOS employing specific inhibitors of either complex I or III of the electron transport chain might impact aerobic glycolysis. Indeed, OXPHOS inhibition by the complex I inhibitor rotenone or the complex III inhibitor antimycin A did result in an impairment of aerobic glycolysis, therefore indicating that aerobic glycolysis at least to some extent depends on preserved OXPHOS activity, providing further evidence of the close

relationship between both pathways of energy generation in activated T cells (Fig. 3 K).

Differential metabolic capacities of high- and low-affinity T cells

Following up on our initial observation of affinity-dependent differences in the extent of DHODH-related effects on T cell proliferation, we hypothesized that this phenomenon might be linked to differences in T cell energy metabolism. We therefore compared the metabolic profiles of high-affinity and low-affinity T cells and observed profound differences between OT-I and OT-III T cells both with regard to OXPHOS and aerobic glycolysis. High-affinity $CD8^+$ T cells were shown to display greater capacities for OXPHOS as well as for aerobic glycolysis, respectively (Fig. 4, A and B). Kinetic analysis further revealed that both maximal respiration and glycolytic capacity were more rapidly upregulated in high-affinity $CD8^+$ T cells compared to low-affinity $CD8^+$ T cells (Fig. 4 C). Interestingly, the extent of DHODH-mediated inhibition of OXPHOS was comparable between high-affinity and low-affinity $CD8^+$ T cells, suggesting that the differential susceptibility towards DHODH-mediated effects is rather due to differences in their metabolic capacity than affinity-differences in DHODH function or relevance (Fig. S5 A). Indeed, a direct comparison of the metabolic capacities of OT-I and OT-III T cells demonstrated that OT-I T cells upregulate OXPHOS and glycolysis under stress, while OT-III T cells increase glycolysis more than OXPHOS (Fig. 4 D). In general, OT-I T cells display a greater energetic capacity compared to OT-III T cells, meaning that OT-III T cells seem to be less dependent on OXPHOS in comparison to OT-I T cells as illustrated by the PhenoGram of OT-I and OT-III T cells 48h after antigen-specific stimulation. Here, OT-III T cells display a strongly limited respiratory capacity compared to OT-I T cells, whereas the difference in glycolytic capacity was less pronounced (Fig. 4 D). Also for $CD4^+$ T cells, high-affinity stimulation resulted in a more pronounced upregulation of OXPHOS as well as glycolysis and ultimately a higher energetic capacity as compared to low-affinity stimulation (Fig. 4, E-G).

Finally, when assessing the function of each respiratory complex separately, OT-I T cells showed a higher complex activity (I-IV) compared to OT-III T cells, again demonstrating that OT-I T cells have a higher OXPHOS ability (Fig. S5 B). In light of the strong dependence of initial T cell proliferation on OXPHOS, this

might explain the distinct inhibitory effect of DHODH inhibition on high-affinity T cell proliferation in comparison to low-affinity T cell proliferation.

Given the affinity-dependent differences in kinetics of energy generation, we next addressed the kinetics of antigen-specific T cell proliferation in high-affinity and low-affinity T cells in more detail. Indeed, high-affinity T cells display a small but crucial kinetic advantage in comparison to low-affinity T cells at early time points, i.e. 36h and 48h after T cell activation, thus mirroring the kinetic differences of energy generation (Fig. 5, A and B). Mechanistically, TCR-derived signals are converted into metabolic activities via a range of key transcription factors serving as intracellular metabolic checkpoints such as IRF4, mTOR or c-Myc *(27, 28)*. We therefore analyzed the expression pattern of these key metabolic transcription factors in high-affinity versus low-affinity T cells early upon TCR-mediated activation. Interestingly, we observed a more pronounced nuclear expression of IRF4, c-Myc and phospho-S6 ribosomal protein, a downstream target of mTOR, in OT-I versus OT-III T cells upon stimulation (Fig. 5, C-E). Of note, DHODH inhibition did not affect IRF4, c-Myc and phospho-S6 ribosomal protein, neither in high-affinity nor in low-affinity T cells (Fig. 5, C-E).

As these data suggest that affinity-dependent intracellular signals are routed into discrete transcriptional networks via modulation of several key transcription factors serving as checkpoints of metabolic T cell programming, we next compared the transcriptional profile of high-affinity and low-affinity T cells with regard to a broad range of metabolically relevant genes in more detail. Importantly, we observed profound differences in the expression levels of numerous metabolically relevant genes in activated high-affinity versus low-affinity T cells as depicted by principal component analysis and scatter plot, respectively (Fig. 5, F and G; Fig. S5, C-E). Interestingly, these differences were only present upon T cell activation (Fig. 5, F and G; Fig. S5, C-E). Moreover, as expected, DHODH inhibition itself did not affect gene expression of metabolically relevant genes (Fig. 5, F and G). Finally, we observed that in total, 53 out of 168 investigated metabolic genes were affinity-dependent, and the majority (48 out of 53) of those were also dependent on TCR stimulation (Fig. 5 H, Table S2).

Together, these data indicate that affinity-dependent signals via the TCR are intracellularly translated into distinct metabolic programs via distinct modulation of a set of key metabolic transcription factors, which in turn result in a differential metabolic capacity of high-affinity versus low-affinity T cells.

Pharmacological DHODH inhibition interferes with mitochondrial complex III function

In light of the profound differences between high-affinity and low-affinity T cells with regard to mitochondrial respiratory capacity, we wondered whether this might be due to quantitative differences in mitochondrial content. However, mitochondrial DNA content was not different between high-affinity and low-affinity T cells (Fig. 6 A). These results could be corroborated by immunohistochemical visualization and quantification of mitochondria illustrating equal presence of mitochondria in activated OT-I and OT-III T cells both in the presence or absence of teriflunomide (Fig. 6, B and C).

We next investigated whether DHODH inhibition might directly interfere with the function of individual complexes of the mitochondrial respiratory chain, a hypothesis that is supported by the close proximity of DHODH to the ubiquinone pool located between complexes II and III *(29)*. First, immunohistochemistry analysis of complex IV (COX) activity revealed a significant increase in COX activity upon T cell stimulation, which was significantly less pronounced in the presence of teriflunomide (Fig. 6 D), indicating that pharmacological DHODH inhibition restricts overall OXPHOS capacity. For a more detailed assessment of individual complexes of the respiratory chain, we measured the activity of mitochondrial complexes I, II/III and IV of the respiratory chain by using intact cells that were first permeabilized and then analyzed using the Agilent Seahorse technology. Here, OT-I T cells were activated in the presence or absence of teriflunomide as previously. After 48h, mitochondrial complexes were successively blocked using specific inhibitors. Measurement of oxygen consumption rate (OCR) revealed that upon inhibition of complexes I to III, OXPHOS was decreased by teriflunomide, while the difference was abolished after substrate supplementation of complex IV, indicating that teriflunomide blocks mitochondrial respiration at complex III (Fig. 6 E).

Taken together, these data illustrate that DHODH inhibition functionally interferes with complex III activity of the electron transport chain in activated T cells, but does not affect mitochondrial content or structure.

DHODH inhibition exerts affinity-dependent effects on effector T cells in vivo

Given the profound affinity-dependent effects of DHODH inhibition in our *in vitro* model systems we then aimed to evaluate whether such affinity-dependent effects might also occur *in vivo* in the context of T cell-mediated autoimmunity. To this end we made use of an established animal model of MS, where mice were immunized with the major histocompatibility complex (MHC) class II MOG_{35-55} peptide and received oral treatment throughout disease course with either leflunomide, the precursor of teriflunomide, or vehicle. In accordance with the literature *(25, 30, 31)*, EAE disease course was significantly ameliorated under leflunomide treatment (Fig. 7 A), accompanied by a strong reduction of infiltrating $CD4^+$ T cell numbers - including those of cytokine producing cells - in the CNS (Fig. 7, B and C). Matching our observations from the TERIDYNAMIC study, absolute numbers of IFNγ-producing $CD4^+$ T cells in the periphery were significantly reduced under leflunomide, whereas numbers of IL-17A producing $CD4^+$ T cells were not affected (Fig. 7 D). When studying different murine Treg subpopulations in these EAE mice under leflunomide, we observed a distinct increase in the subpopulation of Tr1 cells in the circulation, whereas other Treg subpopulations were not affected by leflunomide treatement (Fig. S5 F).

To specifically follow antigen-specific T cells during EAE, we performed tetramer stainings of myelin-specific $CD4^+$ T cells by using the MOG_{35-55} IA^b tetramer. Indeed, we observed a significant reduction in the frequency of MOG-specific $CD4^+$ T cells in the CNS from leflunomide-treated mice (Fig. 7 E). Following this line, we aimed to investigate the antigen-affinities of MOG-specific T cells within the CNS and made use of an elegant method to quantify affinities of antigen-specific T cell responses employing 2D-microscopy as described previously *(32, 33)*. At day 10 after EAE induction, immune cells were isolated from the CNS of these mice and single isolated $CD4^+$ T cells were subjected to 2D microscopy; at least 26 cells per group (w/o n=26, +LF n=28; neg. ctrl n=4) were analyzed in a blinded fashion. Importantly, the adhesion frequency of $CD4^+$ T cells to

MOG_{35-55}-loaded MHC class II molecules as a direct correlate to antigen-affinities was significantly reduced in leflunomide-treated EAE mice compared to vehicle-treated EAE mice (Fig. 7 F). A more detailed analysis further revealed that this significant decrease in mean antigen-affinities in leflunomide-treated mice was mainly driven by the ablation of high-affinity MOG-specific $CD4^+$ T cells (Fig. 7 G). As these data indicate that DHODH inhibition has an impact on the affinity-spectrum of autoreactive T cells *in vivo*, we aimed to translate this finding to the human situation. Here, we made use of a published set-up *(34, 35)* allowing detection of myelin-specific $CD4^+$ T cells by DRB1*0401/MOG_{97-109} and DRB1*0401/$PLP_{180-199}$ tetramer staining in HLA-$DR4^+$ RRMS patients before and during teriflunomide treatment. Importantly, teriflunomide treatment reduced the frequency of MOG- and PLP-specific T cells in the subset of treatment-naïve HLA-$DR4^+$ RRMS patients available to us (Fig. 7, H and I). Together, these data demonstrate that pharmacological DHODH inhibition indeed preferentially affects high-affinity T cells during an antigen-specific autoimmune response *in vivo.*

RRMS patients are characterized by an altered metabolic profile of activated T cells

Finally, we aimed to address the potential relevance of DHODH-mediated metabolic alterations in human RRMS patients. When comparing the metabolic profile of activated $CD4^+$ T cells from RRMS patients and HCs we observed that T cells from RRMS patients during relapse (n=24) but not in the absence of disease activity (n=25), exhibit an enhanced OXPHOS as well as glycolytic activity as compared to HCs (n=24) (Fig. 8, A and B), suggesting that during disease activity, T cells exhibit a disturbed metabolic profile. Along this line, activation-induced increase in mitochondrial respiratory activity as well as glycolysis, as reflected by the relative increase in OCR and ECAR upon T cell stimulation, further illustrates the enhanced metabolic potential of these T cells (Fig. 8, C and D). Again, these metabolic changes were exclusively observed in T cells from patients with an ongoing RRMS relapse. We next investigated the metabolic profile of $CD4^+$ T cells in RRMS patients after teriflunomide treatment. Indeed, we observed a trend towards diminished OXPHOS and aerobic glycolysis in teriflunomide-treated RRMS patients (Fig. 8, E and F), and the same trend was observed in $CD8^+$ T cells (Fig. S6, A). Furthermore, addition of teriflunomide *in vitro* inhibited both OXPHOS and aerobic

glycolysis in activated human T cells both from HCs and RRMS patients (n=10 per group) (Fig. 8, G and H; Fig. S6, B-E).

Taken together, these data suggest that T cells from active RRMS patients exhibit an augmented cellular metabolism, which might contribute to the known immune dysregulation in MS and which is amenable to pharmacological DHODH inhibition.

Discussion

Here, we demonstrate that pharmacological interference with DHODH, a mitochondrial enzyme in the pyrimidine-synthesis pathway and the target of therapeutic agents used for treatment of rheumatoid arthritis and MS, does not uniformly suppress proliferation of activated T cells but instead exerts distinct effects on different T cell clones, which is mainly determined by the affinities of antigen-specific T cell responses and its associated distinct metabolic profiles.

The data from our TERIDYNAMIC trial point towards a rather selective effect of the anti-proliferative drug teriflunomide on different T cell populations, which was somewhat unexpected, as it is generally believed that teriflunomide and leflunomide interfere with the proliferation of any activated T cell due to the increased pyrimidine demand during activation-induced T cell proliferation *(8, 11, 36)*. The preferential reduction in Th1 effector cells by DHODH inhibition not only in human patients but also in the EAE model is intriguing, especially in light of their acknowledged role in autoimmunity *(37–39)*. In support of these *ex vivo* findings we observed an inhibition of murine Th1 cell polarization and proliferation *in vitro* by teriflunomide (Fig. S 7, A and B). On the other hand, absolute iTreg numbers were unaffected resulting in a relative increase in the proportions of iTreg cells within the CD4 compartment and hence an increased iTreg/Th1 ratio, potentially indicating that DHODH inhibition in RRMS patients might restore a disturbed balance between proinflammatory versus anti-inflammatory $CD4^+$ T cell populations. Of note, a relative increase in Tregs upon DHODH inhibition has also been described in other mouse models of autoimmunity *(40–42)*. On a functional level, teriflunomide treatment did neither affect the suppressive capacity of Tregs nor modulate expression of

key regulatory molecules and cytokines, indicating that DHODH is not implicated in the regulation of Treg function itself.

Based on the hypothesis that the observed selective effects of DHODH inhibition on distinct T cell populations might result in TCR repertoire changes, we assessed the effect of teriflunomide treatment on the TCR repertoire in RRMS patients. Interestingly, analysis of our patient cohort revealed that RRMS patients display an enhanced TCR repertoire diversity as illustrated by increased numbers of unique clones and an increased sample overlap. Our findings support pilot data from de Paula Alves Sousa and coworkers *(43)* in a small cohort of five RRMS patients and together suggest that in MS there is a perturbation of clonal elimination, potentially caused by an impaired deletion of autoreactive clones *(44–47)*. It would be of interest to obtain more information about the TCR repertoire in the target organ, i.e. the CNS or at least the CSF, however, it is difficult to obtain CSF in a longitudinal fashion as part of a clinical study and was not included in our study protocol. The pilot study by de Paula Alves Sousa and coworkers indeed pointed towards an enrichment of highly expanded T cell clones in the CSF of RRMS patients, but an analysis of larger cohorts is needed for corroboration. Interestingly, treatment of RRMS patients with teriflunomide resulted in a reduction of TCR repertoire diversity back to the levels of HCs. Although this remains speculative, the preferential sparing of regulatory T cells by teriflunomide might help to restore their capacity to restrict TCR repertoire diversity by elimination of potentially autoreactive T cell clones *(48)*. Of note TCR sequencing does not provide any information about the antigen-specificity or antigen-affinity of the T cell clones investigated, however, the reduction in clonal diversity points to a deletion of distinct clones as a consequence of teriflunomide treatment. Our analysis of myelin-specific $CD4^+$ T cell responses in HLA-$DR4^+$ individuals (Fig. 7, G and H) further supports this concept as we observed a reduction in frequencies of myelin-specific T cells in the course of teriflunomide treatment, albeit this analysis could only be performed in a small subset of patients.

Experiments in preclinical models revealed that DHODH inhibition differentially inhibited T cell proliferation depending on the antigen-affinity of the T cell, as high-affinity T cells were more affected than low-affinity T cells. Recently, Man *et al.* could demonstrate that affinity-dependent signals from the TCR in the context of

infections are translated into distinct transcriptional programs, which in turn determine the metabolic function of effector T cells *(27)*. In light of these data combined with the spatial relationship of DHODH with components of the respiratory chain, we evaluated the impact of DHODH inhibition on key metabolic functions of T cells. During T cell activation, mitochondrial respiration and aerobic glycolysis are both upregulated, and particularly mitochondrial respiration is essential for initial activation of naïve T cells *(18)*. Our data revealed a so far unappreciated role of DHODH in mitochondrial respiration during T cell activation, as DHODH inhibition strongly interfered with OXPHOS in activated but not resting T cells. Furthermore, mitochondrial respiration is particularly important during the first 24h of T cell activation, but – at least in terms of proliferation – is dispensable later on, which is also supported by others *(19)*. While the suppressive effect of DHODH inhibition on mitochondrial respiration is plausible due to the intimate spatial relationship of DHODH with complex III of the respiratory chain, the inhibition of glycolysis was somewhat unexpected. We therefore investigated whether functional mitochondrial respiration *per se* might be a prerequisite for functioning of glycolysis in activated T cells. Indeed, strong inhibition of mitochondrial respiration using complex I and III inhibitors likewise impaired aerobic glycolysis, hence suggesting that the observed drop in glycolytic rate upon DHODH inhibition is most likely indirectly due to its impairment of mitochondrial respiration.

Comparison of metabolic profiles of activated high-affinity and low-affinity T cells revealed significant differences both with regard to transcriptional regulators such as IRF4, c-Myc and the mTOR pathway and transcriptional regulation of metabolic genes. Furthermore, a functional comparison of the metabolic capacities of high- versus low-affinity T cells displayed a clear metabolic advantage of high-affinity T cells both with respect to OXPHOS and aerobic glycolysis. Together, these data do not only provide mechanistic insight into the molecular mechanisms of how TCR signals that result from antigen-specific interactions of certain affinities can be translated into distinct intracellular programs, but also explain the differential effect of DHODH inhibition on high-affinity and low-affinity T cells: Irrespective of antigen-affinities, DHODH inhibition interferes with mitochondrial respiration; however, as high-affinity T cells depend more on mitochondrial

respiration for optimal energy supply during the initial steps of T cell activation, they are more susceptible to signals interfering with mitochondrial respiration such as DHODH inhibition.

With regard to the *in vivo* relevance of the observed affinity-dependent effects of DHODH inhibition, analysis of the antigen-affinity spectrum of MOG-reactive T cell clones in the MOG-induced EAE model provides further evidence that DHODH-mediated affinity-dependent effects are also present in the context of a polyclonal immune response. Importantly, they illustrate that DHODH-inhibition indeed shapes the affinity spectrum of an autoantigen-response, as we observed a preferential ablation of high-affinity MOG-specific T cells in the CNS of leflunomide-treated EAE mice. It has been described that self-reactive T cells with relatively high avidity can escape thymic negative selection and contribute to autoimmune disease manifestation *(13, 14, 49)*. Interestingly, development of organ-specific autoimmunity in a model of diabetes was driven by affinity maturation of the prevailing autoantigen-specific T cell population, and selective depletion of high-affinity T cells prevented disease development *(13)*. These studies underline the relevance of high-affinity T cell clones for disease initiation and progression in different organ-specific autoimmune diseases. Based on these considerations, we propose that during chronic autoimmune responses characterized by repetitive (re-)activation of autoreactive T cells, DHODH inhibition might prevent affinity maturation and hence reduce disease propagation due to its preferential inhibition of high-affinity T cell clones.

From a more general perspective, the relevance of DHODH-dependent changes in T cell metabolism highlights the attractiveness of the concept of immune metabolism as novel therapeutic target in human autoimmune diseases. This concept has been fueled by several experimental studies demonstrating that modulation of immune metabolism can shape immune responses and thus ameliorate autoimmunity in different animal models *(17, 50–52)*. One intriguing example is the illustration of differential metabolic demands of effector versus regulatory T cell subsets *(52–54)*. In this line, we could demonstrate that Th1 cells display a larger capacity for OXPHOS as well as glycolysis compared to Th17 cells, which might render them more susceptible towards DHODH-mediated effects (Fig. S7 C). Intriguingly, although Tregs have been described to employ OXPHOS

for energy generation, a direct comparison of the metabolic properties of resting versus activated Tregs and Th1 cells revealed that although Th1 cells displayed a generally increased glycolytic activity as compared to Tregs, upon activation the rise in OXPHOS activity is more pronounced in Th1 cells, at least *in vitro* (Fig. S7 D). Together, these specific metabolic features of distinct T cell subsets indirectly support our findings of a preferential effect of DHODH inhibition on Th1 cells as opposed to Th17 and Treg populations *in vivo*.

In the context of approved immune-modulatory MS drugs, it has recently been demonstrated that dimethyl fumarate downmodulates aerobic glycolysis in activated myeloid and lymphoid cells via inactivation of the glycolytic enzyme glyceraldehyde 3-phosphate dehydrogenase *(55)*, which further supports the idea that therapeutic targeting of immune metabolism represents an attractive treatment concept also in MS. From another angle, these findings raised the idea that human autoimmune diseases might feature distinct perturbations in immune metabolism, which might be amenable to specific pharmacological modulation once fully understood. So far, a few studies have characterized the immune metabolism of T cells in the context of autoimmune diseases, and disturbances have been observed in rheumatoid arthritis and systemic lupus erythematosus, both in which $CD4^+$ T cells are critical drivers of disease pathogenesis *(56)*. Interestingly, these studies revealed disease-specific differences in T cell immune-metabolism, suggesting that there is no common "autoimmune signature" of immune-metabolic disturbance, but rather distinct alterations, which will require tailored strategies for each disease.

In MS, the focus has been mainly on metabolic disturbances within the CNS, especially in neurons and axons, and mitochondrial injury as well as changes in glucose-metabolizing enzymes have been described in active MS lesions *(57–59)*. In peripheral immune cells from RRMS patients, a pilot study suggested that immune cells from RRMS patients might exhibit altered activities in several complexes of the electron transport chain as well as key enzymes of glycolysis such as hexokinase I pointing towards an impaired mitochondrial respiration and concomitantly decreased glycolytic activity; however, the patient cohort investigated was rather small and active and stable patients were not separately investigated *(16, 60)*. Another study described impaired OXPHOS and glycolysis in activated PBMCs from RRMS patients *(61)*; however, using whole PBMCs for metabolic

measurements does not provide information about the metabolic capacities of individual immune cell subsets. Our study showed that isolated $CD4^+$ T cells from active RRMS patients suffering from an acute relapse exhibit increased mitochondrial respiratory as well as glycolytic activity compared to those of clinically stable RRMS patients and HCs. This intriguing finding has two important implications. First, it supports the notion that T cell-mediated autoimmune diseases are indeed characterized by distinct metabolic alterations, and the metabolic profile seems to be unique to the individual disease pathogenesis. Second, it appears that metabolic alterations in T cells from RRMS patients indeed correlate with disease activity, which will be addressed in more detail in the future.

Together, therapeutic targeting of metabolic alterations might represent an attractive concept in MS and might represent a novel, as yet unrecognized key mechanism of teriflunomide-mediated immune-modulation in this disease.

Materials and Methods

Participants and study design of the TERIDYNAMIC study

TERIDYNAMIC was an exploratory, open-label, phase 3b, clinical trial that recruited patients with RRMS (n=50) from 9 sites in Belgium, Germany, and the Netherlands. All age- and sex-matched HCs (n=20) were recruited from 1 site in Germany. Eligible subjects were 18–56 years of age and met the McDonald 2010 criteria for RRMS. Patients with RRMS were either naive to disease-modifying treatments (DMT), received no DMT for ≥2 years, or received interferon-β (IFNβ) or glatiramer acetate (GLAT) therapy (with ≤3 months of interruption) with a period of ≥2 weeks without IFNβ or GLAT (Table S1). Patients with RRMS were excluded if they experienced a relapse within 30 days prior to screening, had other relevant diseases, were pregnant, breastfeeding, or were of childbearing potential and not utilizing effective birth control. RRMS patients were also excluded if they had previous or concomitant use of cytokine therapy or intravenous immunoglobulins with 3 months of screening, fingolimod within 1 year of screening, natalizumab or other immunosuppressive agents within 2 years of screening, or had ever used alemtuzumab or cladribine. After up to 4 weeks of screening, RRMS patients received 14 mg teriflunomide orally, once a day for 6 months. All subjects who discontinued treatment underwent an accelerated elimination procedure as per local labeling. Follow-ups occurred 4 weeks after treatment discontinuation. Age- and sex-matched HCs (reference group) remained untreated during the screening (up to 1 week) and study period (6 month).

The protocol and its amendments were reviewed and approved by an independent ethics committee (2016-053-f-S). This trial was conducted in accordance with the Declaration of Helsinki and was registered on ClinicalTrials.gov (NCT01863888). All participants provided written informed consent prior to entering the study.

Study subjects independent from the TERIDYNAMIC trial

An independent cohort of 14 treatment-naïve RRMS patients and 10 matched HCs were analyzed for TCR Deep Sequencing (Table S3). Furthermore, a separate cohort of 56 RRMS patients before and during teriflunomide treatment was characterized (Table S4-9). In addition treatment-naïve RRMS patients before and during treatment with dimethyl fumarate (DMF) for 6 months (n=14), IFNβ for 1 year (n=10) or GLAT for 1 year (n=10) were analyzed (Table S10). For human T cell metabolism a total of 59 RRMS patients (stable: n=35; relapse: n=24) and 34 matched HCs were investigated (Table S11 and S12). Stable disease was defined as absence of novel clinical symptoms and no MRI activity within at least 4 weeks prior to PBMC collection. Relapse was defined according to acknowledged clinical criteria, e.g. new or deteriorating of neurological symptoms which last for at least 24h in the absence of infection. Moreover, the characteristics of freshly isolated versus frozen PBMCs were investigated in a cohort of 23 HCs (Table S13 and S14).

Blood sampling of MS patients with clinically definite RRMS according to the McDonald criteria, as well as age- and sex-matched healthy controls (HCs), was approved by the local ethics committee (2010-262-f-S) and all subjects signed informed consent.

Cell Isolation and Immune Cell Phenotyping

Whole blood samples were obtained from all participants at baseline, and at month 3 and 6. Peripheral blood mononuclear cells (PBMCs) were isolated by Ficoll® (Sigma-Aldrich Inc., St Louis, MO, USA) density gradient centrifugation and analyzed by flow cytometry. Adaptive immune cell subsets were identified using the following markers *(62–67)*:

Th1: $CD14^-CD3^+CD56^-CD4^+CD8^-CD45RA^-CD194^-CD196^-CD183^+$

Th2: $CD14^-CD3^+CD56^-CD4^+CD8^-CD45RA^-CD194^+CD196^-CD183^-$

Th17: $CD14^-CD3^+CD56^-CD4^+CD8^-CD45RA^-CD194^+CD196^+CD161^+CD146^+$

Treg: $CD3^+CD56^-CD4^+CD8^-FoxP3^+CD127^{low}$

nTreg: $CD3^{+}CD56^{-}CD4^{+}CD8^{-}FoxP3^{+}CD127^{low}Helios^{+}$

iTreg: $CD3^{+}CD56^{-}CD4^{+}CD8^{-}FoxP3^{+}CD127^{low}Helios^{-}$

To identify potential differences between PBMCs isolated from fresh blood and frozen PBMCs with regard to immune cell subset composition as well as immune functions, an intensive immune cell phenotyping was performed from 12 HCs and analyzed side by side (Fig. S8 A, Table S13). Flow cytometric analysis revealed a remarkably similar pattern of immune cell subsets in fresh versus frozen samples with only minor differences in some subsets.

As expected cytokine production was slightly but significantly diminished in frozen as compared to fresh $CD4^{+}$ T cells. Importantly, longitudinal analysis of a quality control specimen derived from one healthy individual isolated at one time point and stored for different intervals between 0 and 12 months before analysis revealed no detectable impact of freezing duration for a period of 12 months (Fig. S8 B). Detailed analysis of the metabolic properties of freshly isolated versus frozen $CD4^{+}$ T cells were also addressed in a cohort of healthy individuals (Fig. S8 C, Table S14) and did not reveal any significant differences in the metabolic properties of fresh versus frozen cells as determined by Agilent/Seahorse technology.

For detailed description see Supplementary Materials.

TCR Deep Sequencing

CDR3 sequences from $CD4^{+}$ and $CD8^{+}$ T-cell receptor β chains were analyzed by deep sequencing as previously described *(68)*. In brief, mRNA from $CD4^{+}$ T cells isolated from PBMCs was purified and reverse transcribed into cDNA. The TCRβ chain was then amplified by multiplex PCR using primers specific for all 54 known expressed Vβ and all 13 Jβ regions and then deep sequenced by ImmunoSEQ™ (Adaptive Biotechnologies Corp., Seattle, WA, USA). The raw data were annotated according to the IMGT database (LeFranc, Developmental & Comparative Immunology, 2003) and subsequently analyzed with the ImmunoSEQ™ Analyzer software. Global repertoire properties, including the numbers of unique clones and sample overlap, were examined. The term unique clones describes the number of individual clones in a sample.

Sample overlap, the proportion of clones with shared sequences, was calculated as Σ (total numbers of productive reads common to all samples)/total number of productive from all samples.

Since the numbers of unique clones directly correlate with the sequencing depth of each sequencing run, the number can - for pure technical reasons - vary between different runs. Only cohorts sequenced at the same time point or with a similar sequencing depth were compared with each other in order to avoid any technical influences.

Mice

C57BL/6, OT-I transgenic mice responding to Kb/$OVA_{257-264}$ *(69, 70)*, OT-III TCR transgenic mice (provided by Dietmar Zehn, Technical University of Munich) responding with low avidity to Kb/$OVA_{257-264}$ *(24)* and 2D2 TCR transgenic responding to IAb/MOG_{35-55} (low affinity) *(71)* and to IAb/NFM_{15-35} (high affinity) *(21, 22)* were maintained under specific pathogen–free conditions. All animal experiments were performed according to the guidelines of the animal ethics committee and were approved by the government authorities of Nordrhein-Westfalen, Germany (AZ 84-02.04.2017.A073).

Isolation, purification of mouse immune cells

OT-I and OT-III $CD8^+$ T cells or 2D2 $CD4^+$ T cells from spleen and lymph nodes were enriched using positive MACS selection for $CD8^+$ or $CD4^+$ T cells (Miltenyi Biotech) according to the manufacturer's instructions. Splenocytes from C57BL/6 mice were isolated and irradiated with 30 Gy for the antigen-specific stimulation of OT-I and OT-III $CD8^+$ T cells. For antigen-specific stimulation of 2D2 $CD4^+$ T cells dendritic cells (DC) were isolated using positive MACS selection for $CD11b^+$ cells (Miltenyi Biotech) from spleens of C57BL/6 mice according to the manufacturer's instructions.

In vitro cultures of murine cells

OT-I and OT-III $CD8^+$ T cells or 2D2 $CD4^+$ T cells were activated either polyclonally with 4 µg/ml α-CD3 mAb (145-1C11) and 0.5 µg/ml α-CD28 mAb (37.51) (Biolegend) or antigen-specifically. For antigen-specific activation OT-I and OT-III $CD8^+$ T cells were stimulated with irradiated splenocytes from C57BL/6 mice loaded with 500 ng/ml, 50 ng/ml or 5 ng/ml $OVA_{257-264}$ altered peptide ligands SIINFEKL (N4), SIIQFEKL (Q4) or SIITFEKL (T4) (EMC microcollections) and cultured for 2 or 3 days. For antigen-specific stimulation of 2D2 $CD4^+$ T cells $CD11c^+$ DC from spleens of C57BL/6 mice were loaded with 10 µM NFM_{15-35} peptide (RRVTETRSSFSRVSGSPSSGF) or MOG_{35-55} peptide (MEVGWYRSPFSRVVHLYRNGK) (EMC microcollections) and cultured for 3 days.

When indicated, the following drug concentrations were used: 10 µM teriflunomide (TF) (Sanofi Genzyme), 50 µM uridine, 50 µM guanosine, 5/10 nM oligomycin, 10 µM brequinar sodium salt hydrate (Bq), 100/10/1 µM mercaptopurine (Mc), 1/0.1/0.01 µM mitoxantrone dihydrochloride (MT) (Sigma-Aldrich).

All cells were cultured in RPMI 1640, supplemented with 10% FCS, 2 mM L-glutamine, 10 mM Hepes, 1 mM sodium pyruvate, 50 µM 2-mercaptoethanol (Life Technologies) and 1% Penicillin-Streptomycin (Sigma-Aldrich).

To evaluate the optimal TF concentration for *in vitro* cell culture assays, dose-dependent experiments were performed (0/1/10/15/20/50 µM TF) in order to identify the most effective and less toxic concentration of TF. Here, $CD8^+$ OT-I cells were activated with α-CD3/28 and proliferation and cell viability was analyzed by flow cytometry at day 3 (Fig. S9 A). Based on functionality and cell viability, 10 µM TF was taken for further experiments.

To exclude potential baseline differences between OT-I and OT-III T cells the TCR densities were examined by using Quantum™ R-PE MESF Kit (Bangs Laboratories) according to the manufacturer's instructions. Indeed, we observed a slight difference in TCR density on the surface (Fig. S9 B). However, when comparing the proliferative response of OT-I and OT-III T cells both towards antigen-specific and α-CD3/28 stimulation, we could not detect any differences here (Fig. S2 C and D, Fig. S9 C) indicating a comparable response rate upon

TCR stimulation with regard to proliferation rate despite differential expression of TCR receptors. Also, there was no difference in activation markers (Fig. S9 D) or costimulatory molecules (Fig. S9 E).

Metabolism assays of murine cells

Measurements of OCR and ECAR were performed with a Seahorse XFp or XF96 Extracellular Flux Analyzer (Agilent Technologies) as described previously *(72)*. Cells were measured in XF Base Medium Minimal DMEM (Agilent Technologies) supplemented with 2 mM Glutamine, 10 mM Glucose or 1 mM Pyruvate (all Sigma-Aldrich). OCR was evaluated under basal conditions and in response to 1 µM oligomycin, 0.6 µM FCCP, and 100 nM rotenone plus 1 µM antimycin A. ECAR was measured under basal conditions and in response to 100 mM Glucose, 1 µM oligomycin and 5 mM 2-desoxy-glucose (all Sigma-Aldrich). For measurement of complex activity, cells were permeabilized with 3 nM XF Plasma Membrane Permeabilizer (PMP) (Agilent Technologies) according to the company's manual. OCR was evaluated as described previously *(73)*. The substrates 10 mM pyruvate and 0.5 mM malate (complex I), 10 mM succinate (complex II/III), 100 µM TMPD and 10 mM ascorbate (complex IV) were used. For inhibition, 2 µM rotenone (complex I) and 2 µM antimycin A (complex III) were used. Assays were analyzed with the Wave Software (Agilent Technologies).

Experimental autoimmune encephalomyelitis

EAE was performed with age and sex matched C57BL/6 mice as previously described *(74, 75)*. MOG_{35-55}-specific $CD4^+$ T cells were isolated from the CNS of mice treated orally with 17 mg/kg leflunomide (LF) (20 mg ARAVA, Sanofi-Aventis) or with a vehicle (control) at the disease peak (day 10/14) as described previously *(75)*.

For detailed description see Supplementary Materials.

Micropipette adhesion assay

The 2D affinity was assessed with the micropipette adhesion frequency assay as described previously *(33, 76)*. Briefly, a pMHC-coated red blood cell (RBC) and a T cell were placed on opposing micropipettes and brought into contact by micromanipulation for a controlled contact area (Ac) and time (t). The T cell was retracted at the end of the contact period, and the presence of adhesion was observed microscopically by elongation of the RBC membrane. This contact–retraction cycle was performed 50 times per T cell–RBC pair to calculate an adhesion frequency (Pa). The contact area was kept constant for all experiments so it would not affect the affinity comparison. For each experiment, a mean Pa was calculated based only on T cells that bound specifically to antigen. RBCs were loaded with pMHC monomers MOG_{38-49}-IA^b or control $hCLIP_{103-117}$-IA^b (NIH Tetramer Core Facility). Receptor densities on surface of RBCs and T cells were determined using Quantum™ R-PE MESF Kit (Bangs Laboratories) according to the manufacturer's instructions as previously described *(32, 76)*. RBCs were stained with α-MHC II FITC (M5/114.15.2) and T cells were stained with α-TCRβ PE (H57-587) (Biolegend).

Metabolism assays of human cells

Measurements of OCR and ECAR were performed with a Seahorse XFp or XF96 Extracellular Flux Analyzer (Agilent Technologies). Human T cells were isolated either from fresh blood or from frozen PBMC samples of HCs or RRMS patients and measured in XF Base Medium Minimal DMEM (Agilent Technologies) supplemented with 2 mM Glutamine, 10 mM Glucose or 1 mM Pyruvate (all Sigma-Aldrich). OCR was evaluated under basal conditions and in response to 2 μM oligomycin, 1.5 μM FCCP, and 100 nM rotenone plus 1 μM antimycin A. ECAR was measured under basal conditions and in response to 100 mM Glucose, 2 μM oligomycin and 5 mM 2-desoxy-glucose (all Sigma-Aldrich).

T cells from HCs and RRMS patients (Table S11) were thawed and either left unstimulated or were short-term stimulated with 10 ng phorbol 12-myristate 13-acetate (PMA) (Sigma) and 100 ng Ionomycin (Iono) (Cayman Chemical company) for 2.5h prior measurement of mitochondrial respiration and glycolysis inside the Extracellular Flux Analyzer (Agilent Technologies). Activation-induced increase in mitochondrial respiration

and glycolysis was calculated from cells either left unstimulated or stimulated with PMA/Iono for 2.5h prior measurement of OCR and ECAR (stimulated OCR or ECAR values/unstimulated OCR or ECAR values).

Statistical analysis

The baseline value was compared between patients with RRMS and untreated HCs using a Student's t-test, or a Wilcoxon rank-sum test if strong violations from the Gaussian distribution occurred. The change from baseline to month 3 and 6 was analyzed using a linear mixed model including the respective baseline value and time as fixed effects and a random intercept for the patient. Adjusted least squares means (SE) at month 6 of changes from baseline are presented. To compare values obtained from 2 groups, 2-tailed Student's t-test was performed. To compare values acquired from more than 2 groups, 1-way ANOVA or 2-way ANOVA was performed as indicated.

Further Materials and Methods are described in Supplementary Materials.

Supplementary Materials

TERIDYNAMIC study group

Material and Methods

Fig. S1. Changes on T cell subsets in RRMS patients under teriflunomide treatment

Fig. S2. Influence of teriflunomide on proliferation and cytokine production

Fig. S3. Impact of antigen-affinities and DHODH interference on proliferation

Fig. S4. Metabolic assessment of $CD4^+$ and $CD8^+$ T cells under teriflunomide treatment

Fig. S5. Influence of DHODH inhibition on T cell metabolism, gene expression of OT-I and OT-III T cells and on Treg subpopulations in experimental autoimmune encephalomyelitis

Fig. S6. Metabolism of $CD4^+$ and $CD8^+$ T cells from RRMS patients and healthy controls

Fig. S7. Effects of teriflunomide on murine Th1 differentiation and proliferation and metabolic capacities of Th1 cells versus Th17 and Treg cells

Fig. S8. Comparison of freshly isolated versus frozen PBMC from healthy controls regarding immune cell subset composition and metabolism

Fig. S9. Additional information supporting methodology

Table S1. Demographics and Baseline Disease Characteristics TERIDYNAMIC trial

Table S2. Differentially regulated genes depicted in Fig.5 I

Table S3. Demographics and Baseline Disease Characteristics of healthy controls and treatment-naïve RRMS Patients analyzed for TCR repertoire changes

Table S4. Demographics and Baseline Disease Characteristics of treatment-naïve RRMS Patients before and during teriflunomide treatment analyzed for TCR repertoire changes

Table S5. Demographics and Baseline Disease Characteristics of treatment-naïve RRMS Patients before and during teriflunomide treatment analyzed for immune cell phenotyping

Table S6. Demographics and Baseline Disease Characteristics of RRMS Patients before and during teriflunomide treatment for at least 6 months analyzed for suppressive capacity of Tregs

Table S7. Demographics and Baseline Disease Characteristics of RRMS Patients before and during teriflunomide treatment for at least 6 months analyzed for cytokine expression of Tregs

Table S8. Demographics and Baseline Disease Characteristics of treatment-naïve RRMS Patients before and during teriflunomide treatment for at least 6 months analyzed for myelin specific T cell frequencies

Table S9. Demographics and Baseline Disease Characteristics of treatment-naïve RRMS Patients before and during teriflunomide treatment for at least 6 months analyzed for metabolic activity

Table S10. Demographics and Baseline Disease Characteristics of treatment-naïve RRMS Patients before and during treatment with Dimethyl fumarate (DMF), interferon-β (IFNβ) and glatiramer acetate (GLAT) analyzed for TCR repertoire changes

Table S11. Demographics and Baseline Disease Characteristics of healthy controls and treatment-naïve RRMS Patients analyzed for metabolic activity

Table S12. Demographics and Baseline Disease Characteristics of HCs and RRMS Patients analyzed for metabolic activity after 72h of in vitro stimulation

Table S13. Demographics and Baseline Disease Characteristics of healthy controls analyzed for immune cell phenotyping of freshly isolated versus frozen PBMCs

Table S14. Demographics and Baseline Disease Characteristics of healthy controls analyzed for metabolic differences of T cells isolated from fresh blood or frozen PBMCs

References

1. P. O'Connor, J. S. Wolinsky, C. Confavreux, G. Comi, L. Kappos, T. P. Olsson, H. Benzerdjeb, P. Truffinet, L. Wang, A. Miller, M. S. Freedman, Randomized trial of oral teriflunomide for relapsing multiple sclerosis., *N. Engl. J. Med.* **365**, 1293–1303 (2011).

2. C. Confavreux, P. O. Connor, G. Comi, M. S. Freedman, A. E. Miller, T. P. Olsson, J. S. Wolinsky, T. Bagulho, Oral terifl unomide for patients with relapsing multiple sclerosis (TOWER): a randomised , double-blind , placebo- controlled , phase 3 trial, , 247–256 (2014).

3. V. Mladenovic, Z. Domljan, B. Rozman, I. Jajic, D. Mihajlovic, J. Dordevic, M. Popovic, M. Dimitrijevic, M. Zivkovic, G. Campion, Safety and effectiveness of leflunomide in the treatment of patients with active rheumatoid arthritis. Results of a randomized, placebo-controlled, phase II study., *Arthritis Rheum.* **38**, 1595–1603 (1995).

4. J. S. Smolen, J. R. Kalden, D. L. Scott, B. Rozman, T. K. Kvien, A. Larsen, I. Loew-Friedrich, C. Oed, R. Rosenburg, Efficacy and safety of leflunomide compared with placebo and sulphasalazine in active rheumatoid arthritis: a double-blind, randomised, multicentre trial. European Leflunomide Study Group., *Lancet (London, England)* **353**, 259–266 (1999).

5. F. A. Houssiau, D. D'Cruz, S. Sangle, P. Remy, C. Vasconcelos, R. Petrovic, C. Fiehn, E. de Ramon Garrido, I.-M. Gilboe, M. Tektonidou, D. Blockmans, I. Ravelingien, V. le Guern, G. Depresseux, L. Guillevin, R. Cervera, Azathioprine versus mycophenolate mofetil for long-term immunosuppression in lupus nephritis: results from the MAINTAIN Nephritis Trial., *Ann. Rheum. Dis.* **69**, 2083–2089 (2010).

6. B. Griffiths, P. Emery, V. Ryan, D. Isenberg, M. Akil, R. Thompson, P. Maddison, I. D. Griffiths, A.

Lorenzi, S. Miles, D. Situnayake, L. S. Teh, M. Plant, C. Hallengren, O. Nived, G. Sturfelt, K. Chakravarty, T. Tait, C. Gordon, The BILAG multi-centre open randomized controlled trial comparing ciclosporin vs azathioprine in patients with severe SLE., *Rheumatology (Oxford).* **49**, 723–732 (2010).

7. F. C. Breedveld, J. M. Dayer, Leflunomide: mode of action in the treatment of rheumatoid arthritis., *Ann. Rheum. Dis.* **59**, 841–849 (2000).

8. L. Li, J. Liu, T. Delohery, D. Zhang, C. Arendt, C. Jones, The effects of teriflunomide on lymphocyte subpopulations in human peripheral blood mononuclear cells in vitro, *J. Neuroimmunol.* **265**, 82–90 (2013).

9. H. Munier-Lehmann, P.-O. Vidalain, F. Tangy, Y. L. Janin, On dihydroorotate dehydrogenases and their inhibitors and uses., *J. Med. Chem.* **56**, 3148–3167 (2013).

10. A. Bar-Or, H. Wiendl, B. Miller, M. Benamor, P. Truffinet, M. Church, F. Menguy-Vacheron, Randomized study of teriflunomide effects on immune responses to neoantigen and recall antigens., *Neurol. Neuroimmunol. neuroinflammation* **2**, e70 (2015).

11. A. Bar-Or, A. Pachner, F. Menguy-Vacheron, J. Kaplan, H. Wiendl, Teriflunomide and its mechanism of action in multiple sclerosis., *Drugs* **74**, 659–674 (2014).

12. M. Jaberi-Douraki, M. Pietropaolo, A. Khadra, Continuum model of T-cell avidity: Understanding autoreactive and regulatory T-cell responses in type 1 diabetes., *J. Theor. Biol.* **383**, 93–105 (2015).

13. A. Amrani, J. Verdaguer, P. Serra, S. Tafuro, R. Tan, P. Santamaria, Progression of autoimmune diabetes driven by avidity maturation of a T-cell population., *Nature* **406**, 739–742 (2000).

14. B. Han, P. Serra, J. Yamanouchi, A. Amrani, J. F. Elliott, P. Dickie, T. P. Dilorenzo, P. Santamaria, Developmental control of CD8 T cell-avidity maturation in autoimmune diabetes., *J. Clin. Invest.* **115**, 1879–1887 (2005).

15. R. Thomas, M. Turner, A. P. Cope, High avidity autoreactive T cells with a low signalling capacity through the T-cell receptor: central to rheumatoid arthritis pathogenesis?, *Arthritis Res. Ther.* **10**, 210 (2008).

16. N. J. MacIver, R. D. Michalek, J. C. Rathmell, Metabolic regulation of T lymphocytes., *Annu. Rev. Immunol.* **31**, 259–283 (2013).

17. G. D. Norata, G. Caligiuri, T. Chavakis, G. Matarese, M. G. Netea, A. Nicoletti, L. A. J. O'Neill, F. M. Marelli-Berg, The Cellular and Molecular Basis of Translational Immunometabolism., *Immunity* **43**, 421–434 (2015).

18. C.-H. Chang, J. D. Curtis, L. B. J. Maggi, B. Faubert, A. V Villarino, D. O'Sullivan, S. C.-C. Huang, G. J. W. van der Windt, J. Blagih, J. Qiu, J. D. Weber, E. J. Pearce, R. G. Jones, E. L. Pearce, Posttranscriptional control of T cell effector function by aerobic glycolysis., *Cell* **153**, 1239–1251 (2013).

19. G. J. W. van der Windt, D. O'Sullivan, B. Everts, S. C.-C. Huang, M. D. Buck, J. D. Curtis, C.-H. Chang, A. M. Smith, T. Ai, B. Faubert, R. G. Jones, E. J. Pearce, E. L. Pearce, CD8 memory T cells have a bioenergetic advantage that underlies their rapid recall ability., *Proc. Natl. Acad. Sci. U. S. A.* **110**, 14336–41 (2013).

20. J. C. U. Lehmann, J. J. Listopad, C. U. Rentzsch, F. H. Igney, A. von Bonin, H. H. Hennekes, K. Asadullah, W.-D. F. Docke, Dimethylfumarate induces immunosuppression via glutathione depletion and subsequent induction of heme oxygenase 1., *J. Invest. Dermatol.* **127**, 835–845 (2007).

21. L. E. Lucca, S. Desbois, A. Ramadan, A. Ben-Nun, M. Eisenstein, N. Carrie, J.-C. Guery, A. Sette, P. Nguyen, T. L. Geiger, L. T. Mars, R. S. Liblau, Bispecificity for myelin and neuronal self-antigens is a common feature of CD4 T cells in C57BL/6 mice., *J. Immunol.* **193**, 3267–3277 (2014).

22. K. M. Rosenthal, L. J. Edwards, J. J. J. Sabatino, J. D. Hood, H. A. Wasserman, C. Zhu, B. D. Evavold, Low 2-dimensional CD4 T cell receptor affinity for myelin sets in motion delayed response kinetics., *PLoS One* **7**, e32562 (2012).

23. D. Zehn, S. Y. Lee, M. J. Bevan, Complete but curtailed T-cell response to very low-affinity antigen., *Nature* **458**, 211–4 (2009).

24. S. Enouz, L. Carrie, D. Merkler, M. J. Bevan, D. Zehn, L. Carrié, D. Merkler, Autoreactive T cells bypass negative selection and respond to self-antigen stimulation during infection, *J Exp Med* **209**, 1769–1779 (2012).

25. T. Korn, T. Magnus, K. Toyka, S. Jung, Modulation of effector cell functions in experimental autoimmune encephalomyelitis by leflunomide-- mechanisms independent of pyrimidine depletion, *J Leukoc.Biol.* **76**, 950–960 (2004).

26. P. Dimitrova, A. Skapenko, M. L. Herrmann, R. Schleyerbach, J. R. Kalden, H. Schulze-Koops, Restriction of De Novo Pyrimidine Biosynthesis Inhibits Th1 Cell Activation and Promotes Th2 Cell Differentiation, *J. Immunol.* **169**, 3392–3399 (2002).

27. K. Man, M. Miasari, W. Shi, A. Xin, D. C. Henstridge, S. Preston, M. Pellegrini, G. T. Belz, G. K. Smyth, M. A. Febbraio, S. L. Nutt, A. Kallies, The transcription factor IRF4 is essential for TCR affinity-mediated metabolic programming and clonal expansion of T cells., *Nat. Immunol.* **14**, 1155–1165 (2013).

28. R. A. Saxton, D. M. Sabatini, mTOR Signaling in Growth, Metabolism, and Disease, *Cell* **168**, 960–976 (2017).

29. J. Velez, N. J. Hail, M. Konopleva, Z. Zeng, K. Kojima, I. Samudio, M. Andreeff, Mitochondrial uncoupling and the reprograming of intermediary metabolism in leukemia cells., *Front. Oncol.* **3**, 67 (2013).

30. J. E. Merrill, S. Hanak, S.-F. Pu, J. Liang, C. Dang, D. Iglesias-Bregna, B. Harvey, B. Zhu, K. McMonagle-Strucko, Teriflunomide reduces behavioral, electrophysiological, and histopathological deficits in the Dark Agouti rat model of experimental autoimmune encephalomyelitis., *J. Neurol.* **256**, 89–103 (2009).

31. G. E. Ringheim, L. Lee, L. Laws-Ricker, T. Delohery, L. Liu, D. Zhang, N. Colletti, T. J. Soos, K. Schroeder, B. Fanelli, N. Tian, C. W. Arendt, D. Iglesias-Bregna, M. Petty, Z. Ji, G. Qian, R. Gaur, D. Weinstock, J. Cavallo, J. Telsinskas, K. McMonagle-Strucko, Teriflunomide attenuates immunopathological changes in the dark agouti rat model of experimental autoimmune encephalomyelitis., *Front. Neurol.* **4**, 169 (2013).

32. J. Huang, V. I. Zarnitsyna, 932–936.aoyu Liu, B(1) Huang, J.; Zarnitsyna, V. I.; Liu, B.; Edwards, L. J.; Jiang, N.; Evavold, B. D.; Zhu, C. The Kinetics of Two-Dimensional TCR and pMHC Interactions Determine T-Cell Responsiveness. Nature 2010, 464, L. J. Edwards, N. Jiang, B. D. Evavold, C. Zhu, The kinetics of two-

dimensional TCR and pMHC interactions determine T-cell responsiveness., *Nature* **464**, 932–936 (2010).

33. J. J. Sabatino, J. Huang, C. Zhu, B. D. Evavold, High prevalence of low affinity peptide-MHC II tetramer-negative effectors during polyclonal CD4+ T cell responses., *J. Exp. Med.* **208**, 81–90 (2011).

34. K. Raddassi, S. C. Kent, J. Yang, K. Bourcier, E. M. Bradshaw, V. Seyfert-Margolis, G. T. Nepom, W. W. Kwok, D. A. Hafler, Increased frequencies of myelin oligodendrocyte glycoprotein/MHC class II-binding CD4 cells in patients with multiple sclerosis., *J. Immunol.* **187**, 1039–1046 (2011).

35. Y. Cao, B. A. Goods, K. Raddassi, G. T. Nepom, W. W. Kwok, J. C. Love, D. A. Hafler, Functional inflammatory profiles distinguish myelin-reactive T cells from patients with multiple sclerosis, *Sci. Transl. Med.* **7** (2015), doi:10.1126/scitranslmed.aaa8038.

36. K. Ruckemann, L. D. Fairbanks, E. A. Carrey, C. M. Hawrylowicz, D. F. Richards, B. Kirschbaum, H. A. Simmonds, Leflunomide inhibits pyrimidine de novo synthesis in mitogen-stimulated T-lymphocytes from healthy humans., *J. Biol. Chem.* **273**, 21682–21691 (1998).

37. K. K. Hoyer, W. F. Kuswanto, E. Gallo, A. K. Abbas, Distinct roles of helper T-cell subsets in a systemic autoimmune disease., *Blood* **113**, 389–395 (2009).

38. V. Dardalhon, T. Korn, V. K. Kuchroo, A. C. Anderson, Role of Th1 and Th17 cells in organ-specific autoimmunity., *J. Autoimmun.* **31**, 252–256 (2008).

39. U. Kalinke, M. Prinz, Endogenous, or therapeutically induced, type I interferon responses differentially modulate Th1/Th17-mediated autoimmunity in the CNS., *Immunol. Cell Biol.* **90**, 505–509 (2012).

40. T.-Y. Wang, J. Li, C.-Y. Li, Y. Jin, X.-W. Lu, X.-H. Wang, Q. Zhou, Leflunomide induces immunosuppression in collagen-induced arthritis rats by upregulating CD4+CD25+ regulatory T cells., *Can. J. Physiol. Pharmacol.* **88**, 45–53 (2010).

41. B. Weigmann, E. R. Jarman, S. Sudowe, M. Bros, J. Knop, A. B. Reske-Kunz, Induction of regulatory T cells by leflunomide in a murine model of contact allergen sensitivity., *J. Invest. Dermatol.* **126**, 1524–1533

(2006).

42. G. Qiao, L. Yang, Z. Li, J. W. Williams, J. Zhang, A77 1726, the active metabolite of leflunomide, attenuates lupus nephritis by promoting the development of regulatory T cells and inhibiting IL-17-producing double negative T cells., *Clin. Immunol.* **157**, 166–174 (2015).

43. A. de Paula Alves Sousa, K. R. Johnson, R. Nicholas, S. Darko, D. A. Price, D. C. Douek, S. Jacobson, P. A. Muraro, Intrathecal T-cell clonal expansions in patients with multiple sclerosis, *Ann. Clin. Transl. Neurol.* **3**, 422–433 (2016).

44. C. Schuster, K. D. Gerold, K. Schober, L. Probst, K. Boerner, M.-J. Kim, A. Ruckdeschel, T. Serwold, S. Kissler, The Autoimmunity-Associated Gene CLEC16A Modulates Thymic Epithelial Cell Autophagy and Alters T Cell Selection., *Immunity* **42**, 942–952 (2015).

45. B. D. Coder, H. Wang, L. Ruan, D.-M. Su, Thymic involution perturbs negative selection leading to autoreactive T cells that induce chronic inflammation., *J. Immunol.* **194**, 5825–5837 (2015).

46. Y. Fan, G. Gualtierotti, A. Tajima, M. Grupillo, A. Coppola, J. He, S. Bertera, G. Owens, M. Pietropaolo, W. A. Rudert, M. Trucco, Compromised central tolerance of ICA69 induces multiple organ autoimmunity., *J. Autoimmun.* **53**, 10–25 (2014).

47. J. Xia, H. Wang, J. Guo, Z. Zhang, B. Coder, D.-M. Su, Age-Related Disruption of Steady-State Thymic Medulla Provokes Autoimmune Phenotype via Perturbing Negative Selection., *Aging Dis.* **3**, 248–259 (2012).

48. M. Fontaine, I. Vogel, Y.-R. Van Eycke, A. Galuppo, Y. Ajouaou, C. Decaestecker, G. Kassiotis, M. Moser, O. Leo, Regulatory T cells constrain the TCR repertoire of antigen-stimulated conventional CD4 T cells., *EMBO J.* **37**, 398–412 (2018).

49. A. F. M. Maree, P. Santamaria, L. Edelstein-Keshet, Modeling competition among autoreactive CD8+ T cells in autoimmune diabetes: implications for antigen-specific therapy., *Int. Immunol.* **18**, 1067–1077 (2006).

50. Y. Yin, S.-C. Choi, Z. Xu, D. J. Perry, H. Seay, B. P. Croker, E. S. Sobel, T. M. Brusko, L. Morel,

Normalization of CD4+ T cell metabolism reverses lupus., *Sci. Transl. Med.* **7**, 274ra18 (2015).

51. L. Berod, C. Friedrich, A. Nandan, J. Freitag, S. Hagemann, K. Harmrolfs, A. Sandouk, C. Hesse, C. N. Castro, H. Bahre, S. K. Tschirner, N. Gorinski, M. Gohmert, C. T. Mayer, J. Huehn, E. Ponimaskin, W.-R. Abraham, R. Muller, M. Lochner, T. Sparwasser, De novo fatty acid synthesis controls the fate between regulatory T and T helper 17 cells., *Nat. Med.* **20**, 1327–1333 (2014).

52. V. A. Gerriets, R. J. Kishton, A. G. Nichols, A. N. Macintyre, M. Inoue, O. Ilkayeva, P. S. Winter, X. Liu, B. Priyadharshini, M. E. Slawinska, L. Haeberli, C. Huck, L. A. Turka, K. C. Wood, L. P. Hale, P. A. Smith, M. A. Schneider, N. J. MacIver, J. W. Locasale, C. B. Newgard, M. L. Shinohara, J. C. Rathmell, Metabolic programming and PDHK1 control CD4+ T cell subsets and inflammation., *J. Clin. Invest.* **125**, 194–207 (2015).

53. R. D. Michalek, V. A. Gerriets, S. R. Jacobs, A. N. Macintyre, N. J. MacIver, E. F. Mason, S. A. Sullivan, A. G. Nichols, J. C. Rathmell, Cutting edge: distinct glycolytic and lipid oxidative metabolic programs are essential for effector and regulatory CD4+ T cell subsets., *J. Immunol.* **186**, 3299–3303 (2011).

54. M. Galgani, V. De Rosa, A. La Cava, G. Matarese, Role of Metabolism in the Immunobiology of Regulatory T Cells., *J. Immunol.* **197**, 2567–2575 (2016).

55. M. D. Kornberg, P. Bhargava, P. M. Kim, V. Putluri, A. M. Snowman, N. Putluri, P. A. Calabresi, S. H. Snyder, Dimethyl fumarate targets GAPDH and aerobic glycolysis to modulate immunity., *Science* **360**, 449–453 (2018).

56. Z. Yang, H. Fujii, S. V Mohan, J. J. Goronzy, C. M. Weyand, Phosphofructokinase deficiency impairs ATP generation, autophagy, and redox balance in rheumatoid arthritis T cells., *J. Exp. Med.* **210**, 2119–2134 (2013).

57. D. Mahad, I. Ziabreva, H. Lassmann, D. Turnbull, Mitochondrial defects in acute multiple sclerosis lesions, *Brain* **131**, 1722–1735 (2008).

58. M. E. Witte, J. J. G. Geurts, H. E. de Vries, P. van der Valk, J. van Horssen, Mitochondrial dysfunction: a potential link between neuroinflammation and neurodegeneration?, *Mitochondrion* **10**, 411–418 (2010).

59. P. G. Nijland, R. J. Molenaar, S. M. A. van der Pol, P. van der Valk, C. J. F. van Noorden, H. E. de Vries, J. van Horssen, Differential expression of glucose-metabolizing enzymes in multiple sclerosis lesions., *Acta Neuropathol. Commun.* **3**, 79 (2015).

60. L. De Riccardis, A. Rizzello, A. Ferramosca, E. Urso, F. De Robertis, A. Danieli, A. M. Giudetti, G. Trianni, V. Zara, M. Maffia, Bioenergetics profile of CD4(+) T cells in relapsing remitting multiple sclerosis subjects., *J. Biotechnol.* **202**, 31–39 (2015).

61. C. La Rocca, F. Carbone, V. De Rosa, A. Colamatteo, M. Galgani, F. Perna, R. Lanzillo, V. Brescia Morra, G. Orefice, I. Cerillo, C. Florio, G. T. Maniscalco, M. Salvetti, D. Centonze, A. Uccelli, S. Longobardi, A. Visconti, G. Matarese, Immunometabolic profiling of T cells from patients with relapsing-remitting multiple sclerosis reveals an impairment in glycolysis and mitochondrial respiration., *Metabolism.* **77**, 39–46 (2017).

62. C. E. Zielinski, F. Mele, D. Aschenbrenner, D. Jarrossay, F. Ronchi, M. Gattorno, S. Monticelli, A. Lanzavecchia, F. Sallusto, Pathogen-induced human TH17 cells produce IFN-gamma or IL-10 and are regulated by IL-1beta., *Nature* **484**, 514–518 (2012).

63. S. Eyerich, C. E. Zielinski, Defining Th-cell subsets in a classical and tissue-specific manner: Examples from the skin., *Eur. J. Immunol.* **44**, 3475–3483 (2014).

64. T. Akimova, U. H. Beier, L. Wang, M. H. Levine, W. W. Hancock, Helios expression is a marker of T cell activation and proliferation., *PLoS One* **6**, e24226 (2011).

65. M. Sebastian, M. Lopez-Ocasio, A. Metidji, S. A. Rieder, E. M. Shevach, A. M. Thornton, Helios Controls a Limited Subset of Regulatory T Cell Functions., *J. Immunol.* **196**, 144–155 (2016).

66. A. P. Jones, S. Trend, S. N. Byrne, M. J. Fabis-Pedrini, S. Geldenhuys, D. Nolan, D. R. Booth, W. M. Carroll, R. M. Lucas, A. G. Kermode, P. H. Hart, Altered regulatory T-cell fractions and Helios expression in clinically isolated syndrome: clues to the development of multiple sclerosis., *Clin. Transl. Immunol.* **6**, e143 (2017).

67. A. M. Thornton, P. E. Korty, D. Q. Tran, E. A. Wohlfert, P. E. Murray, Y. Belkaid, E. M. Shevach,

Expression of Helios, an Ikaros transcription factor family member, differentiates thymic-derived from peripherally induced Foxp3+ T regulatory cells., *J. Immunol.* **184**, 3433–3441 (2010).

68. T. Schneider-Hohendorf, H. Mohan, C. G. Bien, J. Breuer, A. Becker, D. Gorlich, T. Kuhlmann, G. Widman, S. Herich, C. Elpers, N. Melzer, K. Dornmair, G. Kurlemann, H. Wiendl, N. Schwab, CD8(+) T-cell pathogenicity in Rasmussen encephalitis elucidated by large-scale T-cell receptor sequencing., *Nat. Commun.* **7**, 11153 (2016).

69. A. M. Didierlaurent, C. Collignon, P. Bourguignon, S. Wouters, K. Fierens, M. Fochesato, N. Dendouga, C. Langlet, B. Malissen, B. N. Lambrecht, N. Garcon, M. Van Mechelen, S. Morel, Enhancement of adaptive immunity by the human vaccine adjuvant AS01 depends on activated dendritic cells., *J. Immunol.* **193**, 1920–1930 (2014).

70. K. A. Hogquist, S. C. Jameson, W. R. Heath, J. L. Howard, M. J. Bevan, F. R. Carbone, T cell receptor antagonist peptides induce positive selection, *Cell* **76**, 17–27 (1994).

71. E. Bettelli, M. Pagany, H. L. Weiner, C. Linington, R. A. Sobel, V. K. Kuchroo, Myelin Oligodendrocyte Glycoprotein–specific T Cell Receptor Transgenic Mice Develop Spontaneous Autoimmune Optic Neuritis, *J. Exp. Med. J. Exp. Med* **00**, 1073–1081 (2003).

72. M. Liebmann, S. Hucke, K. Koch, M. Eschborn, J. Ghelman, A. I. Chasan, S. Glander, M. Schädlich, M. Kuhlencord, N. M. Daber, M. Eveslage, M. Beyer, M. Dietrich, P. Albrecht, M. Stoll, K. B. Busch, H. Wiendl, J. Roth, T. Kuhlmann, L. Klotz, Nur77 serves as a molecular brake of the metabolic switch during T cell activation to restrict autoimmunity, *Proc. Natl. Acad. Sci.* , 201721049 (2018).

73. J. K. Salabei, A. A. Gibb, B. G. Hill, Comprehensive measurement of respiratory activity in permeabilized cells using extracellular flux analysis., *Nat. Protoc.* **9**, 421–438 (2014).

74. L. Klotz, S. Hucke, D. Thimm, S. Classen, A. Gaarz, J. Schultze, F. Edenhofer, C. Kurts, T. Klockgether, A. Limmer, P. Knolle, S. Burgdorf, Increased antigen cross-presentation but impaired cross-priming after activation of peroxisome proliferator-activated receptor gamma is mediated by up-regulation of B7H1., *J.*

Immunol. **183**, 129–136 (2009).

75. S. Hucke, J. Flossdorf, B. Grutzke, I. R. Dunay, K. Frenzel, J. Jungverdorben, B. Linnartz, M. Mack, M. Peitz, O. Brustle, C. Kurts, T. Klockgether, H. Neumann, M. Prinz, H. Wiendl, P. Knolle, L. Klotz, Licensing of myeloid cells promotes central nervous system autoimmunity and is controlled by peroxisome proliferator-activated receptor gamma., *Brain* **135**, 1586–1605 (2012).

76. J. Huang, L. J. Edwards, B. D. Evavold, C. Zhu, Kinetics of MHC-CD8 interaction at the T cell membrane., *J. Immunol.* **179**, 7653–7662 (2007).

77. M. Hansen, T. A. Gerds, O. H. Nielsen, J. B. Seidelin, J. T. Troelsen, J. Olsen, pcaGoPromoter--an R package for biological and regulatory interpretation of principal components in genome-wide gene expression data., *PLoS One* **7**, e32394 (2012).

78. M. E. Ritchie, B. Phipson, D. Wu, Y. Hu, C. W. Law, W. Shi, G. K. Smyth, limma powers differential expression analyses for RNA-sequencing and microarray studies., *Nucleic Acids Res.* **43**, e47 (2015).

79. W. Guo, L. Jiang, S. Bhasin, S. M. Khan, R. H. Swerdlow, DNA extraction procedures meaningfully influence qPCR-based mtDNA copy number determination., *Mitochondrion* **9**, 261–265 (2009).

80. G. R. Campbell, I. Ziabreva, A. K. Reeve, K. J. Krishnan, R. Reynolds, O. Howell, H. Lassmann, D. M. Turnbull, D. J. Mahad, Mitochondrial DNA deletions and neurodegeneration in multiple sclerosis., *Ann. Neurol.* **69**, 481–492 (2011).

81. K. M. Clark, R. W. Taylor, M. A. Johnson, P. F. Chinnery, Z. M. Chrzanowska-Lightowlers, R. M. Andrews, I. P. Nelson, N. W. Wood, P. J. Lamont, M. G. Hanna, R. N. Lightowlers, D. M. Turnbull, An mtDNA mutation in the initiation codon of the cytochrome C oxidase subunit II gene results in lower levels of the protein and a mitochondrial encephalomyopathy., *Am. J. Hum. Genet.* **64**, 1330–1339 (1999).

82. M. Auriemma, T. Brzoska, L. Klenner, V. Kupas, T. Goerge, M. Voskort, Z. Zhao, T. Sparwasser, T. A. Luger, K. Loser, alpha-MSH-stimulated tolerogenic dendritic cells induce functional regulatory T cells and ameliorate ongoing skin inflammation., *J. Invest. Dermatol.* **132**, 1814–1824 (2012).

Acknowledgments: We thank Dietmar Zehn (Technical University Munich, Munich, DE) for providing the OT-III transgenic mice. Moreover, we thank Annika Engbers and Andrea Pabst (University Hospital Münster, Münster DE) for excellent technical assistance.

Funding: This study was funded by the Interdisziplinäres Zentrum für Klinische Forschung (IZKF), Münster (LK2/015/14 to LK) and SFB TR128, Projects A08 (to LK), A09 (to CCG and HW) and Z2 (to HW). The TERIDYNAMIC study was funded by Sanofi Genzyme.

Author contributions:

M.Eschborn, M.Lindner, M.Liebmann, B.T.G., V.P., J.B., M.H., A.S.-M., N.F., J.A., C.J., G.R.C., D.J.M., P.H. and G.N. performed experiments and analyzed data and M.Eschborn and M.Lindner wrote the paper.

N.S., T.S.-H., C.C.G., B.P., D.B., S.G., K.B.B., J.R., T.W., K.L., M.Stoll and M.Eveslage analyzed data.

L.K., S.G.M., V.P., T.T. and A.B.-O. designed the study, analyzed and interpreted data and L.K. wrote the paper.

H.W. designed the overall study, analyzed and interpreted experiments and edited paper.

Competing interests:

L.K.: Compensation for serving on scientific advisory boards (Sanofi Genzyme, Novartis); speaker honoraria and travel support (CSL Behring, Merck Serono, Novartis); research support (Biogen Idec, Novartis).

M.Eschborn: Speaker honoraria and travel support (Sanofi Genzyme).

M.Lindner, M.Liebmann, B.T.G., V.P., J.B., M.H., A.S.-M., N.F., J.A., G.N., B.P., J.R., S.G., T.W., K.B.B., G.R.C., D.J.M., K.L., M.Stoll, M.Eveslage: Nothing to disclose.

C.C.G.: Speaker honoraria and travel support (Bayer HealthCare, Sanofi Genzyme)

C.J.: Travel support (Novartis)

T.S.-H.: Travel support (Biogen, Novartis)

P.H.: Speaker honoraria, travel support and financial research support (Novartis, Merck Serono).

D.B.: Lectures, congress invitation, board participation (Bayer, Biogen, MedDay, Merck, Novartis, Roche, Sanofi-Genzyme and Teva)

N.S.: Travel support (Sanofi Genzyme, Novartis).

S.G.M.: Speaker honoraria, travel support and financial research support (Almirall, Amicus Therapeutics Germany, Bayer Health Care, Biogen, Celgene, Diamed, Genzyme, MedDay Pharmaceuticals, Merck Serono, Novartis, Novo Nordisk, ONO Pharma, Roche, Sanofi-Aventis, Chugai Pharma, QuintilesIMS and Teva).

T.T.: Employee of Sanofi Genzyme.

A.B-O.: Speaking, consultancy fees, and/or grant support (Amplimmune, Biogen Idec, Diogenix, Genentech, Sanofi Genzyme, GSK, Merck/EMD Serono, Novartis, Ono Pharma, Receptos, Roche, Teva Neuroscience).

H.W.: Compensation for serving on scientific advisory boards (Biogen, Evgen, MedDay Pharmaceuticals, Merck Serono, Novartis, Roche Pharma AG, Sanofi Genzyme); speaker honoraria and travel support (Alexion, Biogen, Cognomed, F. Hoffmann-La Roche Ltd., Gemeinnützige Hertie-Stiftung, Merck Serono, Novartis, Roche Pharma AG, Sanofi Genzyme, TEVA, and WebMD Global); compensation as consultant (Abbvie, Actelion, Biogen, IGES, Novartis, Roche, Sanofi Genzyme, and the Swiss Multiple Sclerosis Society).

Table 1

	Lymphocytes	$CD4^+$ T cells	$CD8^+$ T cells	$CD19^+$ B cells	Ratio CD4/CD8
Absolute counts (cells/µl)					
Baseline	**1882.8**(651)	**1036.1**(449.7)	**154.3** (97.7;203.9)	N/A	N/A
Month 6	**1587.9**(451)	**913.9**(383.6)	**118.4** (67.5;233.9)		
Δ from baseline	**-284.94(**47.3)	**-101.14**(30.91)	**-34.7** (-55.5;-5.3)		
P value	**<0.001**	**0.002**	**0.005**		
	Lymphocytes (% PBMC)	**$CD4^+$ T cells (% $CD3^+$ cells)**	**$CD8^+$ T cells (% $CD3^+$ cells)**	**$CD19^+$ B cells (% Lymphocytes)**	**Ratio CD4/CD8**
Percentages					
Baseline	**79.5** (9.1)	**82.9** (74.9;88.2)	**12.5** (8.9;18.6)	**10.6** (7.7;14.9)	**6.8** (4.2;9.9)
Month 6	**76.7** (11.3)	**85.3** (79.1;91.2)	**10.9** (6.7;16.9)	**7.7** (6.4;11.8)	**7.8** (4.8;12.8)
Δ from baseline	**-3.05**(1.43)	**1.6** (-0.5;3.7)	**-1.0** (-3.5;0.4)	**-2.0** (-4.1;0)	**0.6** (-0.2;3.9)
P value	**0.040**	**0.006**	**0.009**	**0.001**	**0.008**

Table 1. Evolution and Change from Baseline in the Percentages and Absolute Counts of Overall Lymphocyte Populations and $CD4^+$ T-Cell Subsets in PBMCs. Per-protocol PD population, people with RRMS treated with 14 mg teriflunomide. PBMCs isolated and analyzed by flow cytometry at baseline and 6 months. Data are represented as mean (SD) or median (IQR). Change from baseline represented as LSM change (SEM) or median (IQR). P values from linear mixed model analysis of month 6 with baseline. IQR: interquartile range, LSM: least squares means.

Fig. 1. $CD4^+$ and $CD8^+$ T cell changes in teriflunomide-treated RRMS patients from the TERIDYNAMIC study

(A, B) Changes in $CD4^+$ T cell subpopulations in patients with relapsing-remitting multiple sclerosis (RRMS) after 3 (3M) and 6 months (6M) of teriflunomide (TF) treatment from the TERIDYNAMIC clinical study (demographic data depicted in Table S1). Box plots represent the interquartile range (IQR) with the horizontal line indicating median and error bars showing maximum and minimum values. P values were calculated from linear mixed model on change from baseline. **(A)** Absolute cell numbers of Th1 (n=32), Th2 (n=32), Th17 (n=32) and total regulatory T cells (Treg, n=37). **(B)** Percentages of inducible Treg (iTreg, n=37) cells. **(C, D)** Global TCR repertoire analysis of $CD4^+$ and $CD8^+$ T cells from HCs (n=10) and treatment-naive RRMS patients (n=14) (demographic data depicted in Table S3). Graphs display numbers of unique clones and sample overlap of $CD4^+$ **(C)** and $CD8^+$ **(D)** T cells. For changes at baseline between HCs and RRMS patients, P values were calculated using a Wilcoxon rank-sum test. **(E, F)** Global TCR repertoire analysis of $CD4^+$ and $CD8^+$ T cells from RRMS patients at baseline and after 3M and 6M of TF treatment (n=15) from the TERIDYNAMIC clinical study. Graphs display numbers of unique clones and sample overlap of $CD4^+$ **(E)** and $CD8^+$ **(F)** T cells. P values were calculated from linear mixed model on change from baseline. **(G, H)** Global TCR repertoire properties of $CD4^+$ T cells from RRMS patients at baseline and upon treatment with dimethyl fumarate (DMF) for 6 months (6M) (n=14), interferon-β (IFNβ) for 12 months (12M) (n=10) and glatiramer acetate (GLAT) for 12M (n=10) (demographic data depicted in Table S10). Graphs display numbers of unique clones **(G)** and sample overlap **(H)**. For changes from baseline and (C), P values were calculated using a paired Student's t-test. Horizontal lines indicate mean and error bars show SEM. *P≤0.05, **P≤0.01, ***P≤0.001.

Fig. 2. Antigen affinity-dependent effect of teriflunomide on $CD4^+$ and $CD8^+$ T cells

(A) Proliferation of $CD4^+$ T cells from 2D2 mice upon stimulation with $NFM_{15–35}$ (high-affinity) and MOG_{35-55} (low-affinity) peptides in presence or absence of teriflunomide (TF) at day 3. Data are representative of 4 independent experiments. **(B)** Percentages of proliferated $CD4^+$ T cells from 2D2 mice upon stimulation with $NFM_{15–35}$ and MOG_{35-55} peptides in presence or absence of TF at day 3 (n=4). **(C)** Absolute cell numbers of proliferated $CD4^+$ T cells from 2D2 mice upon stimulation with $NFM_{15–35}$ and MOG_{35-55} peptides in presence or absence of TF at day 3 (n=4). Data were normalized to cells without treatment. **(D)** Proliferation of OT-I $CD8^+$ T cells upon stimulation with altered peptide ligands of $OVA_{257-264}$ with different affinities: SIINFEKL (N4) > SIIQFEKL (Q4) > SIITFEKL (T4) in presence or absence of TF at day 3. Generation analysis was performed with the FlowJo proliferation tool. Data are representative of 3 independent experiments. **(E)** Percentages of proliferated OT-I $CD8^+$ T cells upon stimulation with N4, Q4 and T4 in presence or absence of TF at day 3 (n=3). **(F)** Absolute cell numbers of proliferated OT-I $CD8^+$ T cells upon stimulation with N4, Q4 and T4 in presence or absence of TF at day 3 (n=3). Data were normalized to cells without treatment. **(G)** Proliferation of OT-I (high-affinity TCR) and OT-III (low-affinity TCR) $CD8^+$ T cells upon stimulation with $OVA_{257-264}$ peptide in presence or absence of TF at day 3. Generation analysis was performed with the FlowJo proliferation tool. Data are representative of 3 independent experiments. **(H)** Percentages of proliferated OT-I and OT-III $CD8^+$ T cells upon stimulation with $OVA_{257-264}$ peptide in presence or absence of TF at day 3 (n=3). **(I)** Absolute numbers of proliferated OT-I and OT-III $CD8^+$ upon stimulation with $OVA_{257-264}$ peptide in presence or absence of TF at day 3 (n=3). Data were normalized to cells without treatment. All data are displayed as mean ± SEM. Statistical analysis was employed by Student's t-test and was defined as *P≤0.05, **P≤0.01, ***P≤0.001.

Fig. 3. Influence of DHODH interference on T cell metabolism

(A) Oxygen Consumption Rate (OCR) of α-CD3/28 stimulated 2D2 $CD4^+$ T cells in presence or absence of teriflunomide (TF) at day 3. Data are representative of 3 independent experiments. **(B)** Bar graph of basal and maximal respiration from unstimulated naïve and α-CD3/28 stimulated 2D2 $CD4^+$ T cells in presence or absence of TF at day 3. Data are representative of 3 independent experiments. **(C)** OCR of α-CD3/28 stimulated OT-I $CD8^+$ T cells in presence or absence of TF at day 2. Data are representative of 3 independent experiments. **(D)** Bar graph of basal and maximal respiration from unstimulated naïve and α-CD3/28 stimulated OT-I $CD8^+$ T cells in presence or absence of TF at day 2. Data are representative of 3 independent experiments. **(E)** Extracellular Acidification Rate (ECAR) of α-CD3/28 stimulated 2D2 $CD4^+$ T cells in presence or absence of TF at day 3. Data are representative of 3 independent experiments. **(B)** Bar graph of glycolysis and glycolytic capacity from unstimulated naïve and α-CD3/28 stimulated 2D2 $CD4^+$ T cells in presence or absence of TF at day 3. Data are representative of 3 independent experiments. **(C)** ECAR of α-CD3/28 stimulated OT-I $CD8^+$ T cells in presence or absence of TF at day 2. Data are representative of 3 independent experiments. **(D)** Bar graph of glycolysis and glycolytic capacity from unstimulated naïve and α-CD3/28 stimulated OT-I $CD8^+$ T cells in presence or absence of TF at day 2. Data are representative of 3 independent experiments. **(I)** Inhibition of proliferation of OT-I $CD8^+$ T cells upon stimulation with $OVA_{257-264}$ peptide in presence of TF added at indicated time points and measured at day 3 (n=3). **(J)** Inhibition of mitochondrial respiration and glycolytic capacity of OT-I $CD8^+$ T cells upon stimulation with $OVA_{257-264}$ peptide in presence of TF added at indicated time points and measured at day 2 (n=3). **(K)** ECAR of α-CD3/28 stimulated OT-I $CD8^+$ T cells at day 3. Rotenone (Rot) and Antimycin A (AA) were added as indicated. Data are representative of 3 independent experiments. (Oligo: Oligomycin, FCCP: Carbonyl cyanide-p-trifluoromethoxyphenylhydrazone, Rot: Rotenone, AA: Antimycin A, Gluc: Glucose, 2-DG: 2-Deoxyglucose). All data are displayed as mean ± SEM. Statistical analysis was employed by Student's t-test and was defined as *P≤0.05, **P≤0.01, ***P≤0.001.

Fig. 4. Impact of teriflunomide on high- versus low-affinity T cell metabolism

(A, B) Oxygen Consumption Rate (OCR) **(A)** and Extracellular Acidification Rate (ECAR) **(B)** of OT-I (high-affinity TCR) and OT-III (low-affinity TCR) $CD8^+$ T cells upon stimulation with $OVA_{257-264}$ peptide at day 2. Bar graphs display OCR of basal respiration and maximal respiration **(A)** or ECAR of glycolysis and glycolytic capacity **(B)**. Data are representative of 3 independent experiments. **(C)** Kinetic analysis of maximal respiration and glycolytic capacity of OT-I and OT-III $CD8^+$ T cells upon stimulation with $OVA_{257-264}$ peptide at indicated time points. Data are representative of 3 independent experiments. **(D)** XF PhenoGram of OT-I and OT-III $CD8^+$ T cells upon stimulation with $OVA_{257-264}$ peptide at day 2. Data are representative of 3 independent experiments. **(E, F)** OCR **(E)** and ECAR **(F)** of 2D2 $CD4^+$ T cells upon stimulation with $NFM_{15–35}$ (high-affinity) and MOG_{35-55} (low-affinity) peptides at day 3. Bar graphs display OCR of basal respiration and maximal respiration **(E)** or ECAR of glycolysis and glycolytic capacity **(F)**. Data are representative of 3 independent experiments. **(G)** XF PhenoGram of 2D2 $CD4^+$ T cells upon stimulation with $NFM_{15–35}$ and MOG_{35-55} peptides at day 3. Data are representative of 3 independent experiments. (Oligo: Oligomycin, FCCP: Carbonyl cyanide-p-trifluoromethoxyphenylhydrazone, Rot: Rotenone, AA: Antimycin A). All data are displayed as mean ± SEM. Statistical analysis was employed by Student's t-test and was defined as *P≤0.05, **P≤0.01, ***P≤0.001.

Fig. 5. Affinity-dependent gene expression

(A) Proliferation of OT-I (high-affinity TCR) and OT-III (low-affinity) $CD8^+$ T cells upon stimulation with $OVA_{257-264}$ peptide at indicated time points. Data are representative of 3 independent experiments. **(B)** Statistical analysis of data depicted in **(A)**. **(C)** Expression of transcription factor IRF4 in the nucleus of OT-I and OT-III $CD8^+$ T cells after antigen-specific activation in presence or absence of teriflunomide (TF) for 3h (n=4). Graph displays Mean Fluorescence Intensity (MFI) analyzed by flow cytometry. **(D)** MFI of c-Myc in the nucleus of OT-I and OT-III $CD8^+$ T cells after antigen-specific activation in presence or absence of TF for 1h (n=3). **(E)** Expression of phosphorylated S6 protein, a downstream target of mTOR, in OT-I and OT-III $CD8^+$ T cells after antigen-specific activation in presence or absence of TF for 3h (n=4). Graph displays MFI analyzed by flow cytometry **(F)** Heat map of the expression of 84 glycolytic and 84 mitochondrial respiration genes assessed in OT-I and OT-III $CD8^+$ T cells after antigen-specific activation for 12h in presence or absence of TF. (**G)** Principal component analysis (PCA) of data depicted in **(F)**. **(H)** Venn diagram of all differentially expressed genes (OT-I versus OT-III). Orange indicates the overlap between TCR affinity–regulated genes and stimulation dependent-regulated genes. All data are displayed as mean ± SEM. Statistical analysis was employed by Student's t-test or 1-way ANOVA (C-E) and was defined as *P≤0.05, **P≤0.01, ***P≤0.001.

Fig. 6. Effect of DHODH inhibition on mitochondrial content and function

(A) Relative mt/nDNA ratio of OT-I (high-affinity TCR) and OT-III (low-affinity TCR) $CD8^+$ T cells upon stimulation with $OVA_{257-264}$ peptide in presence or absence of teriflunomide (TF) at day 2 (n=3). Data were normalized to OT-I w/o. **(B)** OT-I and OT-III $CD8^+$ T cells were activated with α-CD3/28 in presence or absence of TF for 2 days. Cells were stained with DAPI (blue) and Mitotracker green (MT green, green). Scale bars indicate 20 µM. **(C)** Quantification of MT green intensity with Image J software. Dots represent the intensity of single images with the same size and exposure time. **(D)** Immunohistochemistry of complex IV (COX) activity of OT-I $CD8^+$ T cells unstimulated or activated with α-CD3/28 in presence or absence of TF at day 2. Scale bars indicate 10 µM. Graph data display quantification of densitometric mean of individual COX puncta. **(E)** Activity of complexes I, II/III and IV of the mitochondrial respiration chain in OT-I $CD8^+$ T cells activated with α-CD3/28 in presence or absence of TF for 2 days (n=3). Cells were permeabilized before measurement and substrates and inhibitors of mitochondrial respiration chain complexes were successively added. Scheme shows simplified illustration of the mitochondrial respiration chain (complexes I-IV) with all substrates (green) and inhibitors (red). (Rot: Rotenone, Succ: Succinate, AA: Antimycin A, TMPD: Tetramethylphenylendiamin, Asc: Ascorbate). All data are displayed as mean ± SEM. Statistical analysis was employed by Student's t-test (A and C), 1-way ANOVA (D) or 2-way ANOVA (E) and was defined as *P≤0.05, **P≤0.01, ***P≤0.001.

Fig. 7. Relevance of DHODH inhibition *in vivo*

(A) Clinical EAE score of C57BL/6 mice treated orally with leflunomide (LF, precursor of teriflunomide (TF)) or vehicle. Active MOG-EAE was induced in C57BL/6 mice (n = 13 per group) and the clinical disease score was assessed daily. **(B, C)** Absolute numbers of $CD4^+$ T cells **(B)**, $CD4^+$ $IFN\gamma^+$ and $CD4^+$ $IL\text{-}17A^+$ T cells **(C)** from the CNS of immunized mice from **(A)** at day 14 analyzed by flow cytometry. **(D)** Absolute numbers of $CD4^+$ $IFN\gamma^+$ and $CD4^+$ $IL\text{-}17A^+$ T cells from the spleen of immunized mice from **(A)** at day 14 analyzed by flow cytometry. **(E)** Tetramer staining of MOG_{35-55}-IA^{b+} $CD4^+$ T cells isolated from the CNS of immunized mice treated with LF or vehicle at day 14. Y-scatter plot displays statistical analysis (n=7-8/group). **(F, G)** Adhesion frequency of MOG_{35-55}-specific $CD4^+$ T cells isolated from the CNS of mice treated with LF or vehicle at day 10 (n=12/group). T cells were tested for adhesion to MOG_{38-49}-IA^b or negative control $hCLIP_{103-117}$-IA^b. Receptor (R) density was assessed by flow cytometry ($CD4^+$ T cells: 18 R/µm^2, pMHC MOG_{38-49}-IAb: 770 R/µm^2, pMHC $hCLIP_{103-117}$-IA^b: 393 R/µm^2) **(H, I)** Treatment-naïve relapsing-remitting multiple sclerosis (RRMS) patients at baseline and during at least 6 months of TF treatment exhibiting the HLA-$DR4^+$ phenotype (n=3) were analyzed for frequencies of myelin-specific T cells by using DRB1*0401/MOG_{97-109}, DRB1*0401/$PLP_{180-199}$ tetramers and the DRB1*0401/$CLIP_{87-101}$ control tetramer (demographic data depicted in Table S8). FACS plots show one representative example. Bar graphs display the relative ratio of MOG_{97-109}^+ **(H)** or $PLP_{180-199}^+$ **(I)** $CD4^+$ T cells to $CLIP_{87-101}^+$ $CD4^+$

T cells. Data are displayed as mean ± SEM. Statistical analysis was employed by 2-way ANOVA (A) or Student's t-test and was defined as *P≤0.05, **P≤0.01, ***P≤0.001.

Fig. 8. Metabolic profiles of T cells from RRMS patients and healthy controls

(A, B) Basal and maximal respiration **(A)** or glycolysis and glycolytic capacity **(B)** of human $CD4^+$ T cells from healthy controls (HC) (n=24), treatment-naïve relapsing-remitting multiple sclerosis (RRMS) patients without (n=25) and with relapse (n=24) upon short-term stimulation with phorbol 12-myristate 13-acetate (PMA) and Ionomycin (Iono) for 2.5h (demographic data depicted in Table S11). **(C, D)** Activation-induced increase in mitochondrial respiration **(C)** and glycolysis **(D)** was calculated from human $CD4^+$ T cells from the cohort depicted in **(A)** and **(B)** either left unstimulated or upon short-term stimulation for 2.5h with PMA/Iono prior to measurement of Oxygen Consumption Rate (OCR) or Extracellular Acidification Rate (ECAR) (stimulated OCR or ECAR values/unstimulated OCR or ECAR values). **(E)** $CD4^+$ T cells from treatment-naïve RRMS patients at baseline and after at least 6 months of TF treatment (n=14) were analyzed for maximal respiration and glycolytic capacity upon short-term stimulation with PMA/Iono for 2.5h (demographic data depicted in Table S9). **(F)** OCR and ECAR values of $CD4^+$ T cells from one representative treatment-naïve RRMS patient at baseline and during TF treatment from **(E)**. **(G)** Maximal respiration and glycolytic capacity of human $CD4^+$ T cells from HCs (n=10) and RRMS patients (n=10) activated with α-CD3/28 in presence or absence of TF for 3 days (demographic data depicted in Table S12). **(H)** OCR and ECAR values of $CD4^+$ T cells from one representative RRMS patient from **(G)**. (Oligo: Oligomycin, FCCP: Carbonyl cyanide-p-trifluoromethoxyphenylhydrazone, Rot: Rotenone, AA: Antimycin A, Gluc: Glucose, 2-DG: 2-Deoxyglucose). All data are displayed as mean ± SEM. Statistical analysis was employed by 1-way ANOVA (A-D) or Student's t-test (E-G) and was defined as *P≤0.05, **P≤0.01, ***P≤0.001.

Supplementary Materials

TERIDYNAMIC study group

Luisa Klotz[1], Maren Lindner[1], Catharina C Gross[1], Melanie Eschborn[1], Anita Posevitz-Fejfar[1], Andreas Schulte-Mecklenbeck[1], Maria Eveslage[2], Bart Van Wijmeersch[3], Raymond Hupperts[4], Mathias Mäurer[5], Martin Stangel[6], Michael Lang[7], Björn Tackenberg[8], Andreas Lysandropoulos[9], Sven G. Meuth[1], Danny Decoo[10], Sandrine Brette[11], Timothy Turner[12], Amit Bar-Or[13] and Heinz Wiendl[1]

Affiliations:

[1]University Hospital Münster, Münster, Germany

[2]University of Münster, Münster, Germany

[3]Hasselt University, Hasselt, Belgium

[4]Maastricht University, Maastricht, Netherlands

[5]Stiftung Juliuspital Würzburg, Würzburg, Germany

[6]Hannover Medical School, Hanover, Germany

[7]Neuropoint Patient Academy, Ulm, Germany

[8]Philipps University and University Clinics Gießen and Marburg, Germany

[9]Erasme Hospital, Free University of Brussels, Brussels, Belgium

[10]AZ Alma, Sijsele, Belgium

[11]Lincoln, Boulogne-Billancourt, France

[12]Sanofi Genzyme, Cambridge, MA, USA

[12]University of Pennsylvania, Philadelphia, PA, USA

Material and Methods

Flow cytometry and intracellular cytokine staining

All fluorochrome-conjugated mAbs were purchased from Biolegend. Cells were stained as described previously *(74)*. OT-I $CD8^+$ T cells were stained with α-TCR Vα-2 FITC (B20.1) and α-TCRβ 5.1,5.2 PE (MR9-4). OT-III $CD8^+$ T cells were stained with α-CD8a FITC (53-6.7) and α-TCRβ 5.1, 5.2 PE (MR9-4). 2D2 $CD4^+$ T cells were stained with α-CD4 FITC (GK 1.5) and α-TCRβ-11 PE (RR3-15). To assess proliferation, cells were labeled with eFluor670® (eBioscience) according to the manufacturer's instructions. For staining of dead cells, Hoechst 33342® (Thermo Fischer) or 7-AAD (eBioscience) was used.

For staining of transcription factors following antibodies were used: α-c-Myc Alexa Fluor® 647 (Cell Signaling), α-IRF4 Alexa Fluor® 647 (eBioscience), α-phospho-S6 ribosomal protein (Ser235/236) Alexa Fluor® 647 (D57.2.2E, Cell Signaling) (downstream target of mTOR). To evaluate the nuclear IRF4 and c-Myc expression, the MFI of the nuclear plus cytosolic IRF4/c-Myc (Transcription Factor Staining Buffer Set, eBioscience) was substracted from MFI of cytosolic IRF4/c-Myc (BD Cytofix/Cytoperm™ Kit, BD Biosciences) in order to obtain only the nuclear fraction of IRF4 and c-Myc.

For intracellular cytokine release, cells were restimulated with lymphocyte activation cocktail (BD Pharmingen) for 3h. Afterwards $CD8^+$ T cells from OT-I and OT-III mice or $CD4^+$ T cells from 2D2 mice were stained with α-IFNγ APC (XMG1.2) and α-Granzyme B (GB11) APC.

For analysis of effector T cells in the CNS and spleen from immunized mice the following antibodies were used: CD45 FITC (30-F11), CD4 PE (GK1.5), CD11b BV510 (M1/70), IL-17A APC (eBio17B7, eBioscience) and IFNγ BV421 (XMG1.2).

For analysis of Treg subpopulations in the blood and spleen of immunized mice the following antibodies were purchased: CD4 Pacific Blue (GK1.5), CD25 Alexa Fluor® 700 (PC61), CD304 PE (NRP-1, 3E12), Helios FITC (22FG), CD49b PerCP/Cy5.5 (DX5), CD223 APC (LAG-3, C9B7W).

For staining of MOG IA^b-positive $CD4^+$ T cells isolated from the CNS of immunized mice, cells were stained with T-Select I-A^b MOG_{35-55} tetramer-PE (MBL) or without tetramer (negative control), CD4 APC (RM4-5) and CD3 PC5.5 (17A2) after manufactures instructions. Dead cells were discriminated using Hoechst 33342® (Thermo Fischer).

For human immune cell phenotyping of frozen versus freshly isolated PBMC from HCs the following markers were used to determine immune cell subsets:

Lymphocytes: FSC vs SSC, $CD14^-$

B cells: $CD19^+CD3^-$ Lymphocytes

T cells: $CD3^+CD56^-$ Lymphocytes

CD4: $CD4^+CD8^-$ T cells

CD4 HLA-DR^+: HLA-DR^+ CD4

CD4/CD8 naive: $CD45RO^-CD45RA^+CD197^+CD62L^+$

CD4/CD8 memory: $CD45RO^+CD45RA^-$

CD8 TEMRA: $CD45RO^-CD45RA^+CD197^-CD62L^-$ CD8

Treg: $CD45RO^+CD127^{low}FoxP3^+CD25^+$ CD4

pTreg: $Helios^-$ Treg

tTreg: $Helios^+$ Treg

Th1: $CD45RO^+CCR4^-CCR6^-CXCR3^+$ CD4

Th2: $CD45RO^+CCR4^+CCR6^-CXCR3^-$ CD4

Th17: $CD45RO^+CCR4^+CCR6^+CXCR3^-$ CD4

Flow cytometric measurement was performed with a Gallios flow cytometer (Beckman Coulter). Data were analyzed using FlowJo Software (Tree Star).

Cytokine detection with ELISA

Cytokine levels of IFNγ, GM-CSF and TNFα were assessed in the supernatants of T cells isolated from the spleen and lymph nodes of OT-I, OT-III and 2D2 mice after 3 days of antigen-specific activation using Enzyme-Linked Immunosobent Assay (ELISA) Ready Set-Go® (eBioscience) according to the manufacturer's instructions.

RT2-PCR-Profiler PCR Array

OT-I and OT-III $CD8^+$ T cells were antigen-specifically activated for 12h. RNA was isolated using RNeasy Mini Kit (Qiagen) with an integrated DNA digestion on the column using RNase-Free DNase Set (Qiagen) according to the manufacturer's instruction. RNA quality and quantity was assessed using a Nanodrop 1000 Spectrophotometer (Peqlab). cDNA synthesis was performed from total RNA using a RT2FirstStrand Kit (Qiagen). We determined expression of glycolic genes (RT² Profiler™ PCR Array Mouse Glucose Metabolism, #PAMM-006Z) and genes involved in mitochondrial respiration (RT² Profiler™ PCR Array Mouse Mitochondrial Energy Metabolism, #PAMM-008Z) using RT2 Profiler RCR Arrays (Qiagen). Quantitative PCR was carried out on the CFX-384 (BioRad) using RT2 Real-Time SYBR Green PCR Master Mix (SuperArray Bioscience) according to the manufacturer's protocol. As internal controls, two different housekeeping genes b-actin (ACTB) and beta-2-microglobulin (B2m) were used.

Principal Component Analysis was performed on scaled and centered RT2 Profiler array data using the R package pcaGoPromoter version 1.18.0 *(77)*. Dendrograms for heatmap visualization were calculated with Euclidean average clustering and visualized along with scaled and centered data. Differentially expressed genes were determined with the R package limma version 3.30.13 *(78)* as having an FDR-corrected p-value < 0.05 (Benjamini-Hochberg correction) and fold change > 1.5.

Analysis of mtDNA/nDNA content and ratio

Genomic DNA was purified using QIAamp DNA micro Kit (Qiagen) and carried out according to the manufacturer's instructions. The quality and quantity of genomic DNA was assessed with a Nanodrop 1000

Spectrophotometer (Peqlab). MtDNA/nDNA ratios were analyzed as described previously *(79)*. Briefly, the gene expression was determined in triplicates using gene-specific primers for cytochrome c oxidase subunit 1 (CO1) gene of the mtDNA and NADH dehydrogenase ubiquinone flavoprotein 1 (NDUFV1) gene of nDNA. The CO1 primers were 5-TGC TAG CCG CAG GCA TTA C-3 (forward primer) and 5-GGG TGC CCA AAG AAT CAG AAC-3 (reverse primer). The NDUFV1 primers were 5-CTT CCC CAC TGG CCT CAA G-3 (forward primer) and 5-CCA AAA CCC AGT GAT CCA GC-3 (reverse primer). The PCR reaction mixture was prepared with 40 ng/ml genomic DNA and with PowerSYBR Green PCR Master Mix (Applied Biosystems) according to the manufacturer´s protocol. Amplification of genomic DNA was carried out on a StepOnePlusTM System (Applied Biosystems). Data were examined for the ratio of CT values (mtDNA/nDNA).

Imaging

OT-I and OT-III $CD8^+$ T cells were activated with α-CD3/28 in presence or absence of 10 μM teriflunomide for 2 days and stained for Mitotracker Green (final concentration: 100 nM; life technologies) and DAPI (Thermo Scientific) according to the manufacturer's instructions. A confocal laser scanning microscope (Leica SP8) with a tunable white light laser and a laser diode of 405 nm was used for parallel dual color excitation/emission microscopy. Z-stacks of cells were recorded through a motorized 63x objective (HC PL APO 63x/1.20 W motCORR CS2) with 2 HyD SP GaAsP detectors. DAPI was excited with 405 nm, emission range was set between 455 to 469 nm. MitoTracker® Green was excited with 488 nm and emission recorded between 496 nm and 522 nm.

Complex IV (COX) Immunohistochemistry

OT-I $CD8^+$ T cells were either unstimulated or activated with α-CD3/28 in presence or absence of 10 μM teriflunomide (TF) for 2 days. After spin down of cells (75,000) to super frost microscope slides (Thermo Fischer), cells were air dried and stored at -80 °C. Afterwards mitochondrial respiratory chain activity was

analyzed by sequential complex IV (COX) immunohistochemistry as described previously *(80)*. Briefly, slides were air dried for 60 min at room temperature prior incubation in COX medium (100 mM cytochrome c, 4 mM diaminobenzidine tetrahydro-chloride and 20 µg/ml catalase in 0.1 M phosphate buffer, pH 7.0) at 37°C for 50 min *(57, 81)*. Subsequent immunohistochemistry, the sections were dehydrated in 70, 90 and 100% ethanol followed by Histoclear (National Diagnostics, Atlanta, Georgia, USA) and mounted in DPX (Sigma). Finally, brightfield images were taken on an Olympus BX51 microscope at 40x magnification.

Experimental autoimmune encephalomyelitis

EAE was performed as previously described *(74)*. Briefly, age and sex matched C57BL/6 mice were immunized with 50 µg $MOG_{35–55}$ peptide (GL Biochem (Shanghai) Ltd.) emulsified in complete Freund's adjuvant (BD) containing *Mycobacterium tuberculosis.* Two injections of 200 ng Pertussis toxin (Sigma) in PBS were also performed on the day of immunization and two days later. Mice were scored as previously described *(75)*. Briefly, daily clinical assessment of EAE was performed using a scale ranging from 0 to 8: 0, no paralysis; 1, limp tail; 2, ataxia or unilateral hind limb paresis; 3, severe unilateral or weak bilateral hind limb paresis; 4, severe bilateral hind limb paresis; 5, complete bilateral hind limb plegia; 6, complete bilateral hind limb plegia and partial forelimb paresis; 7, severe tetraparesis/plegia; and 8, moribund/dead animals. MOG_{35-55}-specific $CD4^+$ T cells were isolated from the CNS and spleen of mice treated orally with 17 mg/kg leflunomide (LF) (20 mg ARAVA, Sanofi-Aventis) or with a vehicle (control) at the disease peak (day 10/14) as described previously *(75)*.

In vitro differentiation of murine Th1, Th17 and Treg cells

$CD4^+$ T cells were isolated from lymph nodes and spleen of C57/BL6 mice using positive MACS selection (Miltenyi Biotech) according to the manufacturer's instructions. Afterwards $CD4^+$ T cells were stimulated with 4 µg/ml α-CD3/28 and cultured with specific cytokine cocktails to polarize the cells into a Th1, Th17 or Treg phenotype for 3 days (Th1: 10 µg/ml α-IL-4, 20 ng/ml IL-12; Th17: 5 ng/ml TGFβ, 20 ng/ml IL-6, 10 µg/ml α-

IL-4,10 µg/ml α-IFNγ; Treg: 5 ng/ml TGFβ, 10 µg/ml α-IL-4,10 µg/ml α-IFNγ) (IL-12, TGFβ, IL-6 from Prepotech; purified α-IL-4 and α-IFNγ antibodies from Biolegend).

Human Treg suppression assay

Treg and Teff cells were isolated from frozen PBMC of RRMS patients (Table S6) before and during at least 6 months of TF treatment using $CD4^+$ $CD25^+$ Regulatory T Cell Isolation Kit (Miltenyi Biotech) according to the manufacturer's instructions. Subsequently, Teff cells ($CD4^+$ $CD25^-$) were labeled with Carboxyfluorescein Diacetate Succinimidyl Ester (CFSE, Invitrogen) after companies manual. Then Teff cells were cocultured in a 1:1 ratio with or without autologous Treg and stimulated with a-human CD3 (HIT3a, Biolegend) und a-human CD28 (CD28.2, Biolegend) monoclonal antibodies for 5 days as described previously *(82)*. Proliferation was assessed via flow cytometry. Stimulated Teff cells without Treg served as a control.

Cytokine detection with Luminex

Treg were isolated from frozen PBMC of RRMS patients (Table S7) before and during at least 6 months of TF treatment using $CD4^+$ $CD25^+$ Regulatory T Cell Isolation Kit (Miltenyi Biotech) according to the manufacturer's instructions. Then, Treg cells were stimulated with a-human CD3 (HIT3a, Biolegend) und a-human CD28 (CD28.2, Biolegend) monoclonal antibodies for 5 days. The supernatants of these Treg cell cultures were analyzed for cytokine release using a High Sensitivity 9-Plex Human ProcartaPlex™ Panel measured by Luminex MAGPIX® System.

Determination of myelin-specific frequencies of human T cells

PBMCs from three treatment-naïve RRMS patients before and during TF treatment for at least 6 months with the correct HLA-$DR4^+$ genotype (Table S8) were analyzed for myelin-specific frequencies as by Cao et al. *(35)*. PBMCs were loaded with a pool of peptides each 10 µg/ml (MBP_{85-99}, $MOG_{222-241}$, PLP_{30-49}, $PLP_{129-148}$, MOG_{97-109}, $PLP_{180-199}$). Thereafter cells were cultured ($5x10^6$/ml) for 14 days in HL-1 medium containing 5% human

serum. IL-2 (20 U/ml) was added on days 4, 7, and 10. The cultures were split in two wells and supplemented with fresh medium on day 7.

For tetramer staining, the cells were washed with PBS, then stained with 10 mg/ml PE-labeled tetramer (DRB1*0401/$MOG_{97–109}$, DRB1*0401/$PLP_{180-199}$ or control DRB1*0401/$CLIP_{87-101}$) at 37˚C for 3h in HL-1 medium with 2% human serum. Cells were stained for the last 30 min with α-CD19 APC and α-CD4 FITC mAbs (Biolegend); dead cells were discriminated using Zombie AquaTM (Biolegend). Flow cytometry data were analyzed with FlowJo software (Tree Star, Ashland, OR).

Isolation and purification of human T cells for analysis of metabolism

PBMCs were isolated from voluntary RRMS patients and HCs. $CD4^+$ and $CD8^+$ T cells were enriched using positive selection via MACS technology (Miltenyi Biotech) according to the manufacturer's instructions.

In vitro cultures of human T cells for analysis of metabolism

Human $CD4^+$ and $CD8^+$ T cells were activated with 4 µg/ml α-CD3 mAb (OKT3) (Biolegend) and 0.5 µg/ml α-CD28 mAb (CD28.2) (eBioscience) and cultured in X-Vivo Media 15 (Lonza) in presence or absence of 10 µM TF for 3 days (Table S12).

Fig. S1

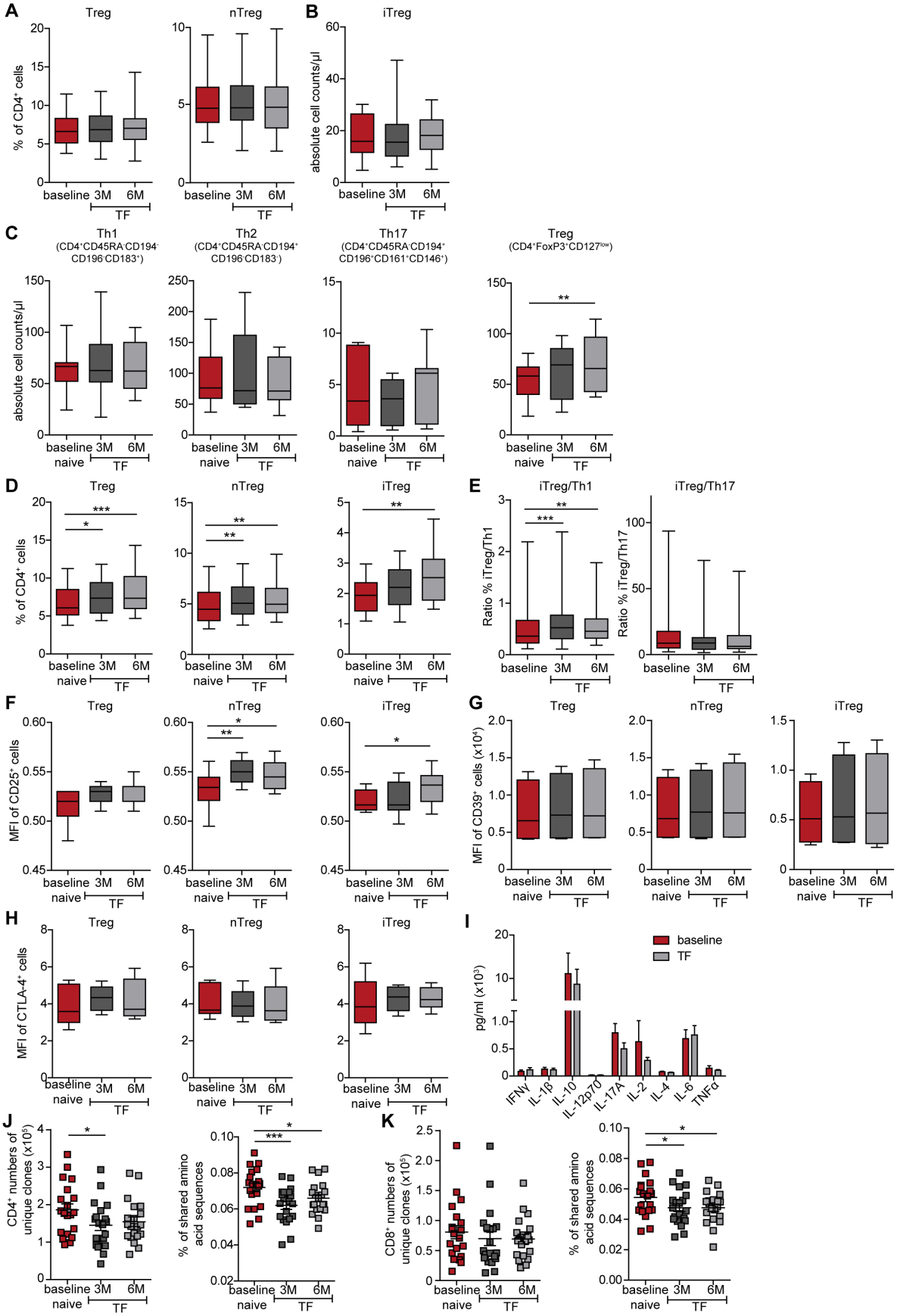
A
Treg
nTreg
% of CD4+ cells
baseline 3M 6M
TF
B
iTreg
absolute cell counts/µl
C
Th1
(CD4+CD45RA-CD194-CD196-CD183+)
Th2
(CD4+CD45RA-CD194+CD196-CD183-)
Th17
(CD4+CD45RA-CD194+CD196+CD161+CD146+)
Treg
(CD4+FoxP3+CD127low)
naive
D
E
iTreg/Th1
iTreg/Th17
Ratio % iTreg/Th1
Ratio % iTreg/Th17
F
MFI of CD25+ cells
G
MFI of CD39+ cells (x10⁴)
H
MFI of CTLA-4+ cells
I
baseline
TF
pg/ml (x10³)
IFNγ
IL-1β
IL-10
IL-12p70
IL-17A
IL-2
IL-4
IL-6
TNFα
J
CD4+ numbers of unique clones (x10⁵)
% of shared amino acid sequences
K
CD8+ numbers of unique clones (x10⁵)

Fig. S1. Changes on T cell subsets in RRMS patients under teriflunomide treatment

(A-B) Changes in $CD4^+$ T cell subpopulations in patients with relapsing-remitting multiple sclerosis (RRMS) after 3 (3M) and 6 months (6M) of teriflunomide (TF) treatment from the TERIDYNAMIC clinical study (demographic data depicted in Table S1). **(A)** Percentages of total regulatory T cells (Treg) (n=37) and natural Treg (nTreg) (n=37) cells. **(B)** Absolute numbers of inducible (iTreg, n=37). **(C, D)** Changes in $CD4^+$ T cell subpopulations in treatment-naïve RRMS patients after 3M and 6M of TF treatment from the TERIDYNAMIC clinical study. **(C)** Absolute numbers of Th1 (n=7), Th2 (n=7), Th17 (n=7) and total Treg cells (n=8) within the $CD4^+$ T cell population. **(D)** Percentages of total Treg (n=8) and subpopulation analysis of nTreg (n=8) and iTreg (n=8). **(E)** Changes in $CD4^+$ T cell subpopulations in RRMS patients after 3M and 6M of TF treatment from the TERIDYNAMIC clinical study. Ratio from percentages of iTreg/Th1 (n=32) and iTreg/Th17 (n=32). **(F, G)** Data from treatment-naïve RRMS patients at baseline and after 3M and 6M of TF treatment (demographic data depicted in Table S5). Mean Fluorescence Intensity (MFI) of CD39 (n=4) **(F)** and CTLA-4 (n=6) **(G)** from total Treg, nTreg and iTreg cell populations. All box plots represent the interquartile range (IQR) with the horizontal line indicating median and error bars showing maximum and minimum values. P values were calculated from linear mixed model on change from baseline. **(H)** Suppressive capacity of Treg isolated from frozen PBMC of RRMS patients before and after at least 6M of TF treatment (n=10) (demographic data depicted in Table S6). Effector T cells from the same donor were cultivated either with autologous Treg or alone and stimulated with α-CD3/28 for 5 days. Proliferation was assessed by flow cytometry. **(I)** Detection of indicated cytokines in the supernatant of Tregs isolated from RRMS patients before and during at least 6M of TF treatment (n=18) (demographic data depicted in Table S7) after α-CD3/28 stimulation for 5 days. **(J, K)** Global TCR repertoire analysis of $CD4^+$ **(J)** and $CD8^+$ **(K)** T cells from treatment-naïve RRMS patients at baseline and after 3M and 6M of TF treatment (n=20) (demographic data depicted in Table S4). Data display numbers of unique clones and sample overlap. P values were calculated from linear mixed model on change from baseline. Horizontal lines indicate mean and error bars show SEM. *P≤0.05, **P≤0.01, ***P≤0.001.

Fig. S2

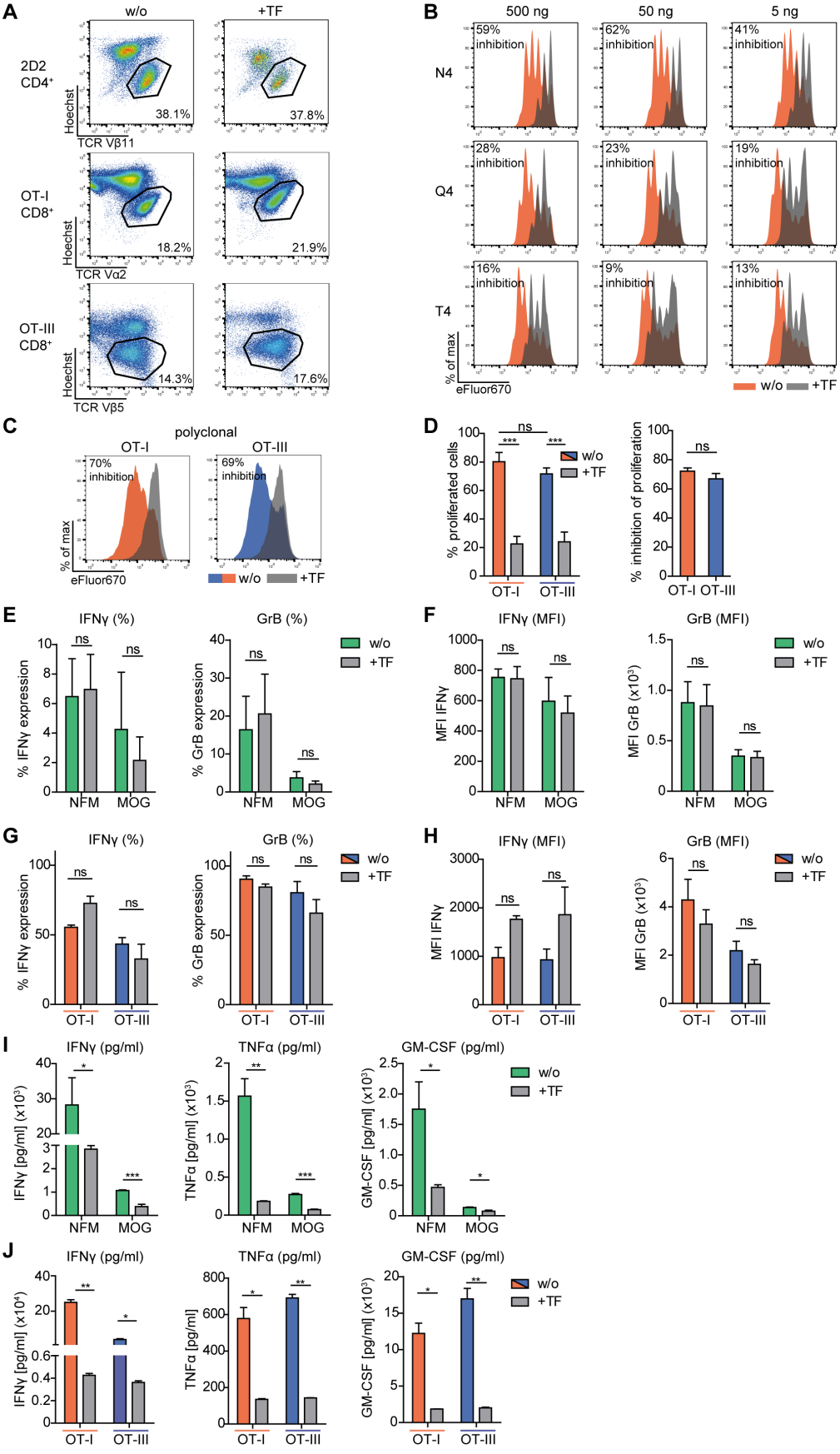
A
w/o
+TF
2D2 CD4+
Hoechst
38.1%
37.8%
TCR Vβ11
OT-I CD8+
18.2%
21.9%
TCR Vα2
OT-III CD8+
14.3%
17.6%
TCR Vβ5
B
500 ng
50 ng
5 ng
N4
59% inhibition
62% inhibition
41% inhibition
Q4
28% inhibition
23% inhibition
19% inhibition
T4
16% inhibition
9% inhibition
13% inhibition
% of max
eFluor670
w/o
+TF
C
polyclonal
OT-I
OT-III
70% inhibition
69% inhibition
D
% proliferated cells
% inhibition of proliferation
ns
***
E
IFNγ (%)
GrB (%)
% IFNγ expression
% GrB expression
NFM
MOG
F
IFNγ (MFI)
GrB (MFI)
MFI IFNγ
MFI GrB (x10³)
G
H
OT-I
OT-III
I
IFNγ (pg/ml)
TNFα (pg/ml)
GM-CSF (pg/ml)
IFNγ [pg/ml] (x10³)
TNFα [pg/ml] (x10³)
GM-CSF [pg/ml] (x10³)
J
IFNγ [pg/ml] (x10⁴)
TNFα [pg/ml]
GM-CSF [pg/ml] (x10³)

Fig. S2. Influence of teriflunomide on proliferation and cytokine production

(A) Viability of $CD4^+$ and $CD8^+$ T cells. 2D2 $CD4^+$ T cells upon α-CD3/28 stimulation and OT-I (high-affinity TCR) as well as OT-III (low-affinity TCR) $CD8^+$ T cells upon stimulation with $OVA_{257-264}$ peptide in presence or absence of teriflunomide (TF) at day 3. For further analysis, Hoechst-negative viable cells were taken. Data are representative of 3 independent experiments. **(B)** Proliferation of OT-I $CD8^+$ T cells upon stimulation with altered peptide ligands of $OVA_{257-264}$ with different affinities: SIINFEKL (N4) > SIIQFEKL (Q4) > SIITFEKL (T4) in presence or absence of TF at day 3. Data are representative of 3 independent experiments. **(C)** Proliferation of OT-I and OT-III $CD8^+$ T cells upon α-CD3/28 stimulation in presence or absence of TF at day 3. Data are representative of 3 independent experiments. **(D)**. Percentages of proliferated cells and inhibition of proliferation of OT-I and OT-III $CD8^+$ T cells upon α-CD3/28 stimulation in presence or absence of TF at day 3 (n=3). **(E, F)** Percentages **(E)** and Mean Fluorescence Intensity (MFI) **(F)** of IFNγ and granzyme B (GrB) expression of 2D2 $CD4^+$ T cells upon stimulation with $NFM_{15–35}$ (high-affinity) and MOG_{35-55} (low-affinity) peptides in presence or absence of TF at day 3 detected via intracellular cytokine staining after restimulation (n=3). **(G, H)** Percentages **(G)** and MFI **(H)** of IFNγ and GrB expression of OT-I and OT-III $CD8^+$ T cells after antigen-specific activation in presence or absence of TF at day 3 detected via intracellular cytokine staining after restimulation (n=3). **(I)** Detection of the cytokines IFNγ, tumor necrosis factor alpha (TNFα) and granulocyte-macrophage colony-stimulating factor (GM-CSF) in the supernatant of 2D2 $CD4^+$ T cells after antigen-specific activation in presence or absence of TF at day 3. Data are representative of 3 independent experiments. **(J)** Detection of the cytokines IFNγ, TNFα and GM-CSF in the supernatant of OT-I and OT-III $CD8^+$ T cells after antigen-specific activation in presence or absence of TF at day 3. Data are representative of 2 independent experiments. All data are displayed as mean ± SEM. Statistical analysis was employed by 1-way ANOVA (D) or Student's t-test (E-J) and was defined as *P≤0.05, **P≤0.01, ***P≤0.001.

Fig. S3

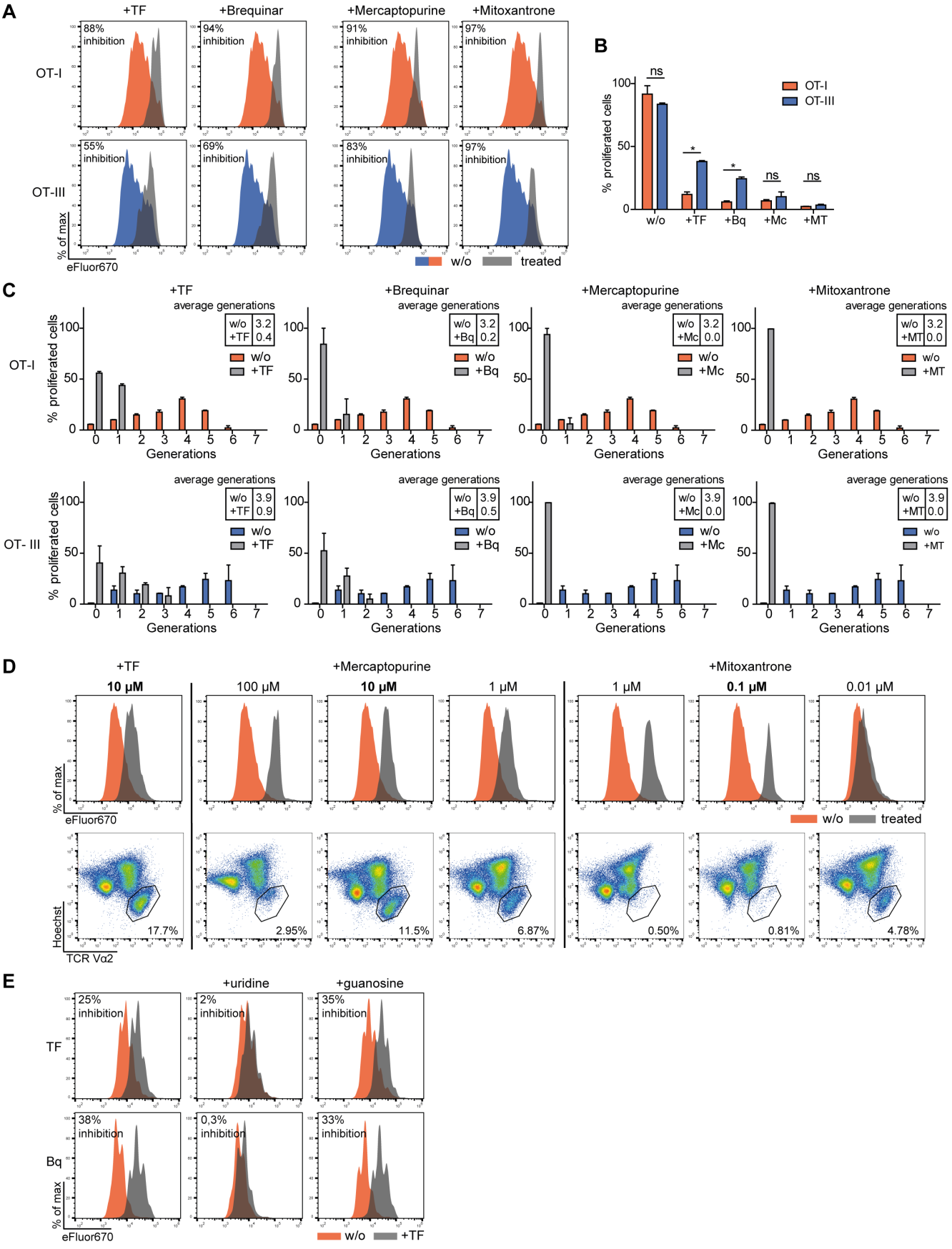
A
+TF
+Brequinar
+Mercaptopurine
+Mitoxantrone
OT-I
OT-III
88% inhibition
94% inhibition
91% inhibition
97% inhibition
55% inhibition
69% inhibition
83% inhibition
97% inhibition
% of max
eFluor670
w/o
treated
B
% proliferated cells
OT-I
OT-III
ns
*
*
ns
ns
w/o
+TF
+Bq
+Mc
+MT
C
+TF
+Brequinar
+Mercaptopurine
+Mitoxantrone
average generations
w/o 3.2
+TF 0.4
+Bq 0.2
+Mc 0.0
+MT 0.0
OT-I
OT- III
% proliferated cells
Generations
w/o
+TF
+Bq
+Mc
+MT
w/o 3.9
+TF 0.9
+Bq 0.5
+Mc 0.0
+MT 0.0
D
+TF
+Mercaptopurine
+Mitoxantrone
10 µM
100 µM
10 µM
1 µM
1 µM
0.1 µM
0.01 µM
% of max
eFluor670
w/o
treated
Hoechst
TCR Vα2
17.7%
2.95%
11.5%
6.87%
0.50%
0.81%
4.78%
E
+uridine
+guanosine
TF
Bq
25% inhibition
2% inhibition
35% inhibition
38% inhibition
0,3% inhibition
33% inhibition
% of max
eFluor670
w/o
+TF

Fig. S3. Impact of antigen-affinities and DHODH interference on proliferation

(A) Proliferation of OT-I (high-affinity TCR) and OT-III (low-affinity TCR) $CD8^+$ T cells upon stimulation with $OVA_{257-264}$ peptide in presence or absence of teriflunomide (TF), brequinar (Bq), mercaptopurine (Mc) or mitoxantrone (MT) at day 3. Data are representative of 3 independent experiments. **(B)** Percentages of proliferated OT-I and OT-III $CD8^+$ T cells after antigen-specific activation in presence or absence of TF, Bq, Mc or MT at day 3 (n=2). **(C)** Generation analysis of proliferated OT-I and OT-III $CD8^+$ T cells after antigen-specific activation in presence or absence TF, Bq, Mc or MT at day 3. Data are representative of one experiment with 3 technical replicates. **(D)** Proliferation profiles and cell viability of OT-I $CD8^+$ T cells after antigen-specific activation in presence or absence of TF, Mc or MT at day 3. Highlighted concentrations were taken for further experiments based on functionality and viability of the cells. **(E)** Proliferation of OT-I and OT-III $CD8^+$ T cells after antigen-specific activation in presence or absence of TF, Bq, uridine or guanosine at day 3. Data are representative of 3 independent experiments. All data are displayed as mean ± SEM. Statistical analysis was employed by Student's t-test and was defined as *P≤0.05, **P≤0.01, ***P≤0.001.

Fig. S4

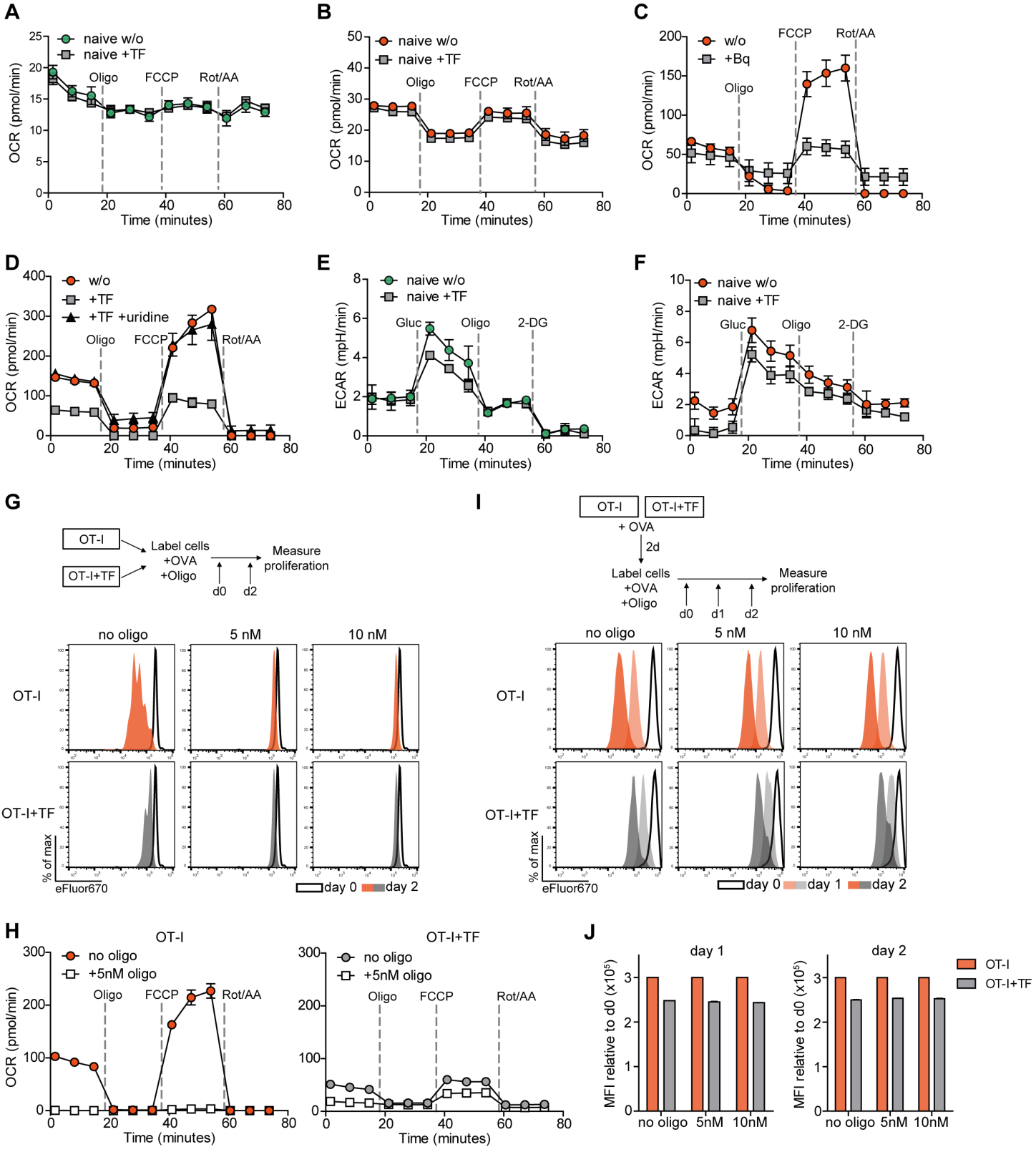
A
naive w/o
naive +TF
Oligo
FCCP
Rot/AA
OCR (pmol/min)
Time (minutes)
B
naive w/o
naive +TF
Oligo
FCCP
Rot/AA
OCR (pmol/min)
Time (minutes)
C
w/o
+Bq
Oligo
FCCP
Rot/AA
OCR (pmol/min)
Time (minutes)
D
w/o
+TF
+TF +uridine
Oligo
FCCP
Rot/AA
OCR (pmol/min)
Time (minutes)
E
naive w/o
naive +TF
Gluc
Oligo
2-DG
ECAR (mpH/min)
Time (minutes)
F
naive w/o
naive +TF
Gluc
Oligo
2-DG
ECAR (mpH/min)
Time (minutes)
G
OT-I
OT-I+TF
Label cells
+OVA
+Oligo
Measure proliferation
d0
d2
no oligo
5 nM
10 nM
OT-I
OT-I+TF
% of max
eFluor670
day 0
day 2
I
OT-I
OT-I+TF
+ OVA
2d
Label cells
+OVA
+Oligo
Measure proliferation
d0
d1
d2
no oligo
5 nM
10 nM
OT-I
OT-I+TF
% of max
eFluor670
day 0
day 1
day 2
H
OT-I
no oligo
+5nM oligo
Oligo
FCCP
Rot/AA
OCR (pmol/min)
Time (minutes)
OT-I+TF
no oligo
+5nM oligo
Oligo
FCCP
Rot/AA
Time (minutes)
J
day 1
MFI relative to d0 (x10^5)
no oligo
5nM
10nM
day 2
MFI relative to d0 (x10^5)
no oligo
5nM
10nM
OT-I
OT-I+TF

Fig. S4. Metabolic assessment of $CD4^+$ and $CD8^+$ T cells under teriflunomide treatment

(A) Oxygen Consumption Rate (OCR) of unstimulated naïve 2D2 $CD4^+$ T cells in presence or absence of teriflunomide (TF) at day 3. Data are representative of 3 independent experiments. **(B)** OCR of unstimulated naïve OT-I $CD8^+$ T cells in presence or absence of TF at day 2. Data are representative of 3 independent experiments. **(C)** OCR of OT-I $CD8^+$ T cells stimulated with α-CD3/28 in presence or absence of brequinar (Bq) at day 2. Data are representative of 3 independent experiments. **(D)** OCR of OT-I $CD8^+$ T cells stimulated with α-CD3/28 in presence or absence of TF and uridine at day 2. Data are representative of 3 independent experiments. **(E)** Extracellular Acidification Rate (ECAR) of unstimulated naïve 2D2 $CD4^+$ T cells in presence or absence of TF at day 3. Data are representative of 3 independent experiments. **(F)** ECAR of unstimulated naïve OT-I $CD8^+$ T cells in presence or absence of TF at day 2. Data are representative of 3 independent experiments. **(G)** Proliferation OT-I $CD8^+$ T cells upon stimulation with $OVA_{257-264}$ peptide in presence or absence of TF and indicated concentrations of oligomycin (oligo) at days 0 and 2. Data are representative of 2 independent experiments. **(H)** OCR of OT-I $CD8^+$ T cells upon stimulation with $OVA_{257-264}$ peptide in presence or absence of oligo and TF at day 2. Data are representative of 2 independent experiments. **(I)** OT-I $CD8^+$ T cells were stimulated with $OVA_{257-264}$ peptide in presence or absence of TF for 2 days. Afterwards cells were labeled with eFluor670 and cultured $OVA_{257-264}$ peptide in presence or absence of oligo for up to 2 days. Data display proliferation at day 0, 1 and 2 after addition of oligo. Data are representative of 2 independent experiments. **(J)** Analysis of proliferation of OT-I $CD8^+$ T cells shown in **(I)**. Graphs indicate Mean Fluorescence Intensity (MFI) relative to d0. Data were normalized to OT-I $CD8^+$ T cells. Data are representative of 2 independent experiments. All data are displayed as mean ± SEM.

Fig. S5

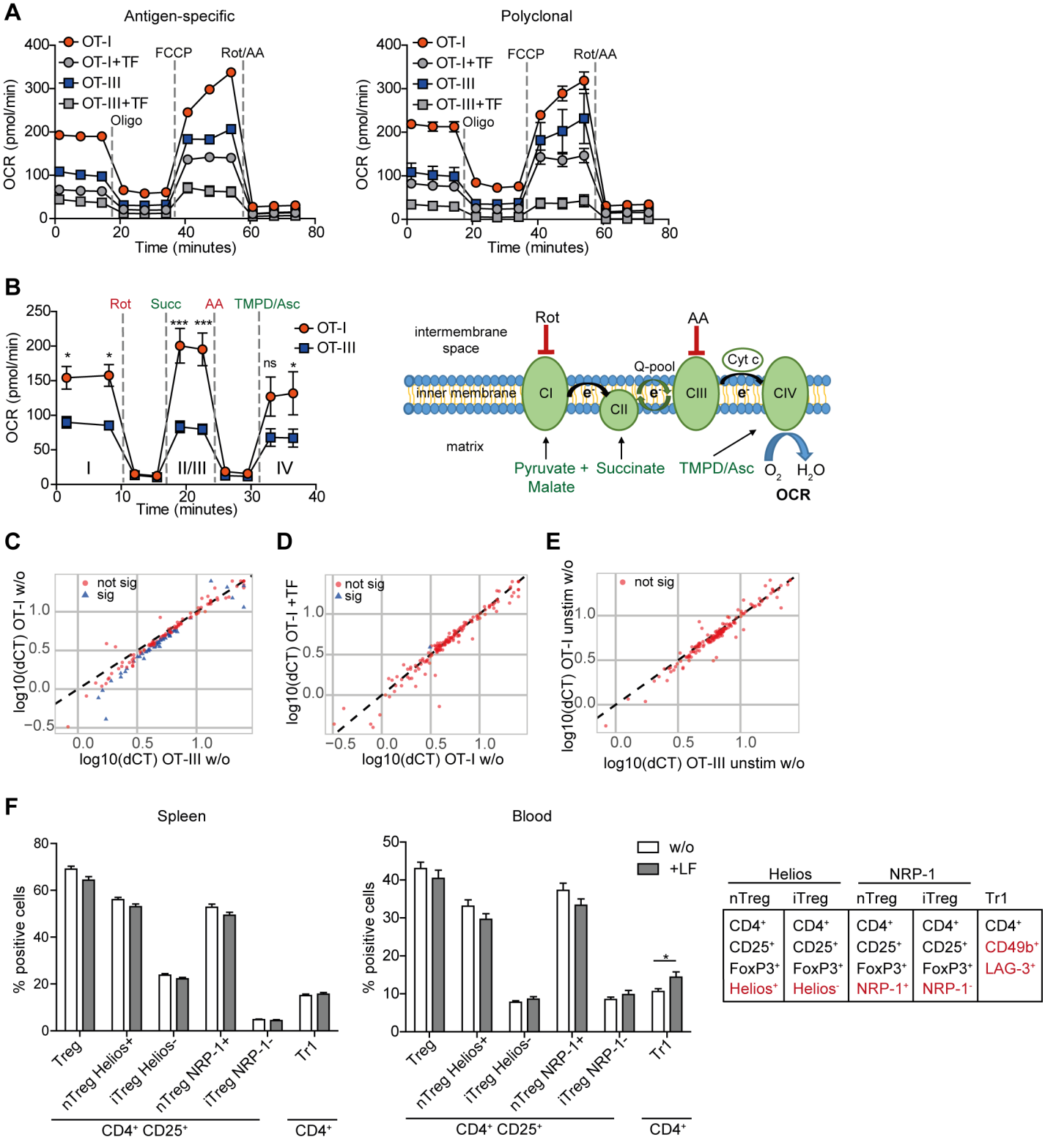

Helios		NRP-1		
nTreg	iTreg	nTreg	iTreg	Tr1
CD4+	CD4+	CD4+	CD4+	CD4+
CD25+	CD25+	CD25+	CD25+	CD49b+
FoxP3+	FoxP3+	FoxP3+	FoxP3+	LAG-3+
Helios+	Helios-	NRP-1+	NRP-1-	

Fig. S5. Influence of DHODH inhibition on T cell metabolism, gene expression of OT-I and OT-III T cells and on Treg subpopulations in experimental autoimmune encephalomyelitis

(A) Mitochondrial respiration of OT-I (high-affnity TCR) and OT-III (low-affinity TCR) $CD8^+$ T cells upon stimulation with either $OVA_{257-264}$ peptide (left) or α-CD3/28 (right) in presence or absence of teriflunomide (TF) at day 2 (n = 3). **(B)** Activity of complexes I, II/III and IV of the mitochondrial respiration chain. OT-I and OT-III $CD8^+$ T cells were activated with α-CD3/28 for 2 days. Cells were permeabilized before measurement and substrates (green) and inhibitors (red) of mitochondrial respiration chain complexes were successively added as indicated (n=3). Scheme shows simplified illustration of mitochondrial respiration chain (complexes I-IV) with all substrates and inhibitors. **(C-E)** Scatterplot of ΔCT values of two independent groups plotted on a log base 10 scale. **(C)** OT-I and OT-III $CD8^+$ T cells upon stimulation with $OVA_{257-264}$ peptide for 12h; blue triangle indicates differentially expressed genes. **(D)** OT-I $CD8^+$ T cells upon stimulation with $OVA_{257-264}$ peptide in presence or absence of TF for 12h. **(E)** Unstimulated OT-I versus OT-III $CD8^+$ T cells. **(F)** Active EAE was induced by $MOG_{35–55}$ immunization in C57BL/6 mice (n = 13 per group) treated with leflunomide (LF, precursor of TF) or vehicle. At day 14 of EAE, spleen and blood was analyzed for regulatory T cell (Treg) markers (Helios, NRP-1, CD49b, LAG-3) by flow cytometry. Treg subpopulations were defined as follows: Treg $CD4^+CD25^+FoxP3^+$, nTreg $CD4^+CD25^+FoxP3^+Helios^+$ or $CD4^+CD25^+FoxP3^+NRP\text{-}1^+$, iTreg $CD4^+CD25^+FoxP3^+Helios^-$ or $CD4^+CD25^+FoxP3^+NRP\text{-}1^-$, Tr1 $CD4^+CD49b^+LAG\text{-}3^+$. (Rot: Rotenone, Succ: Succinate, AA: Antimycin A, TMPD: Tetramethylphenylendiamin, Asc: Ascorbate, Oligo: Oligomycin, FCCP: Carbonyl cyanide-p-trifluoromethoxyphenylhydrazone, Gluc: Glucose, 2-DG: 2-Deoxyglucose). All data are displayed as mean ± SEM. Statistical analysis was employed by 2-way ANOVA (B) or Student's t-test and was defined as *P≤0.05, **P≤0.01, ***P≤0.001.

Fig. S6

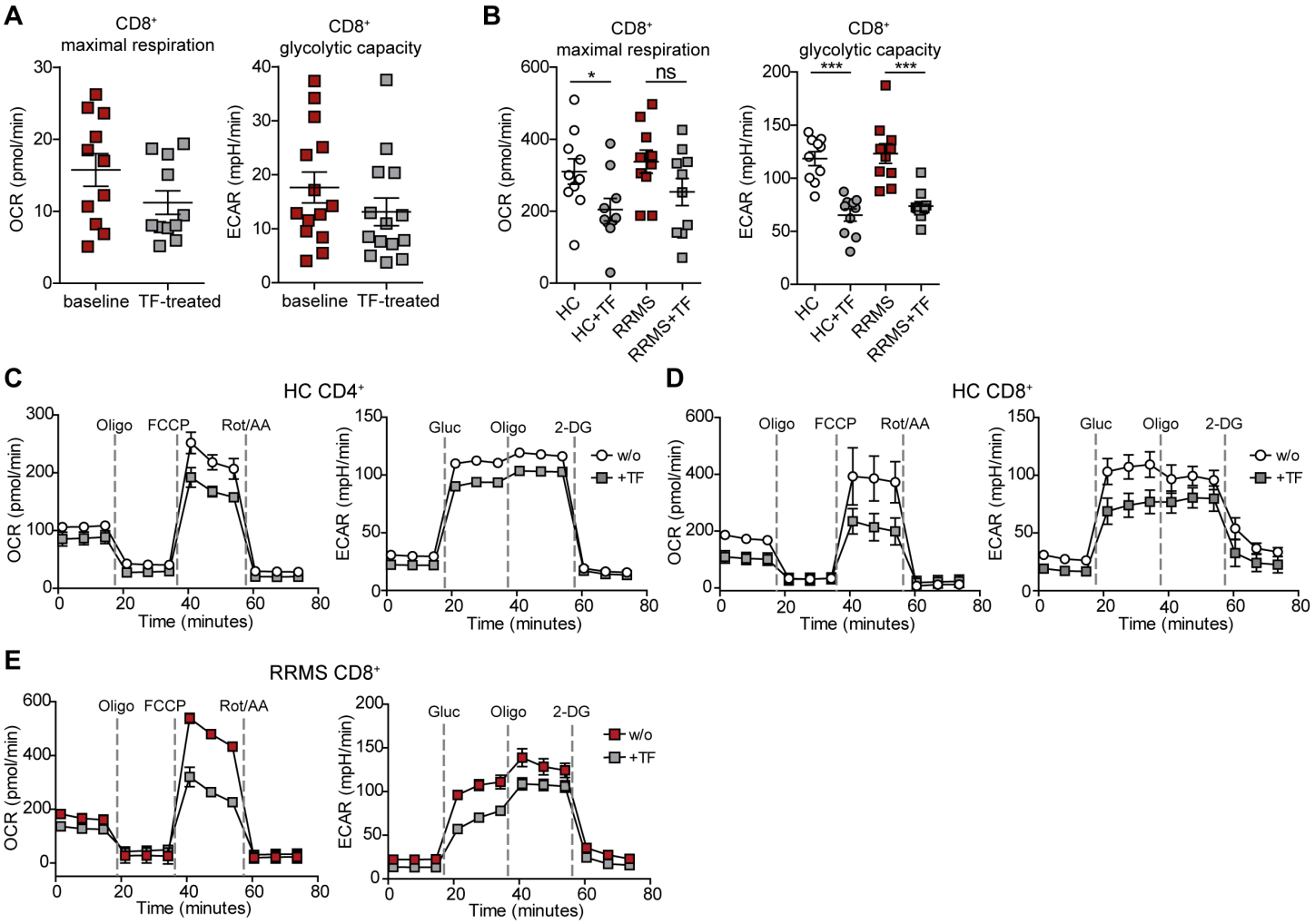

Fig. S6. Metabolism of CD4$^+$ and CD8$^+$ T cells from RRMS patients and healthy controls

(A) Maximal respiration (left) and glycolytic activity (right) of CD8$^+$ T cells isolated from frozen PBMCs from treatment-naïve RRMS patients at baseline and after at least 6 months of TF treatment (n=14). Cells were measured after short-term stimulation with phorbol 12-myristate 13-acetate (PMA) and Ionomycin for 2.5h (demographic data depicted in Table S9). **(B)** Maximal respiration (left) and glycolytic activity (right) of freshly isolated CD8$^+$ T cells from HCs (n=10) and RRMS patients (n=10) 3 days after stimulation with α-CD3/28 in presence or absence of TF (demographic data depicted in Table S12). (**C-E**) Mitochondrial respiration (left) and glycolysis (right) of freshly isolated CD4$^+$ and CD8$^+$ T cells from HCs and RRMS patients 3 days after stimulation with α-CD3/28 in presence or absence of TF (demographic data depicted in Table S12). Data are representative of 10 independent experiments. (Oligo: Oligomycin, FCCP: Carbonyl cyanide-p-trifluoromethoxyphenylhydrazone, Rot: Rotenone, AA: Antimycin A, Gluc: Glucose, 2-DG: 2-Deoxyglucose). All data are displayed as mean ± SEM. Statistical analysis was employed by Student's t-test and was defined as *P≤0.05, **P≤0.01, ***P≤0.001.

Fig. S7

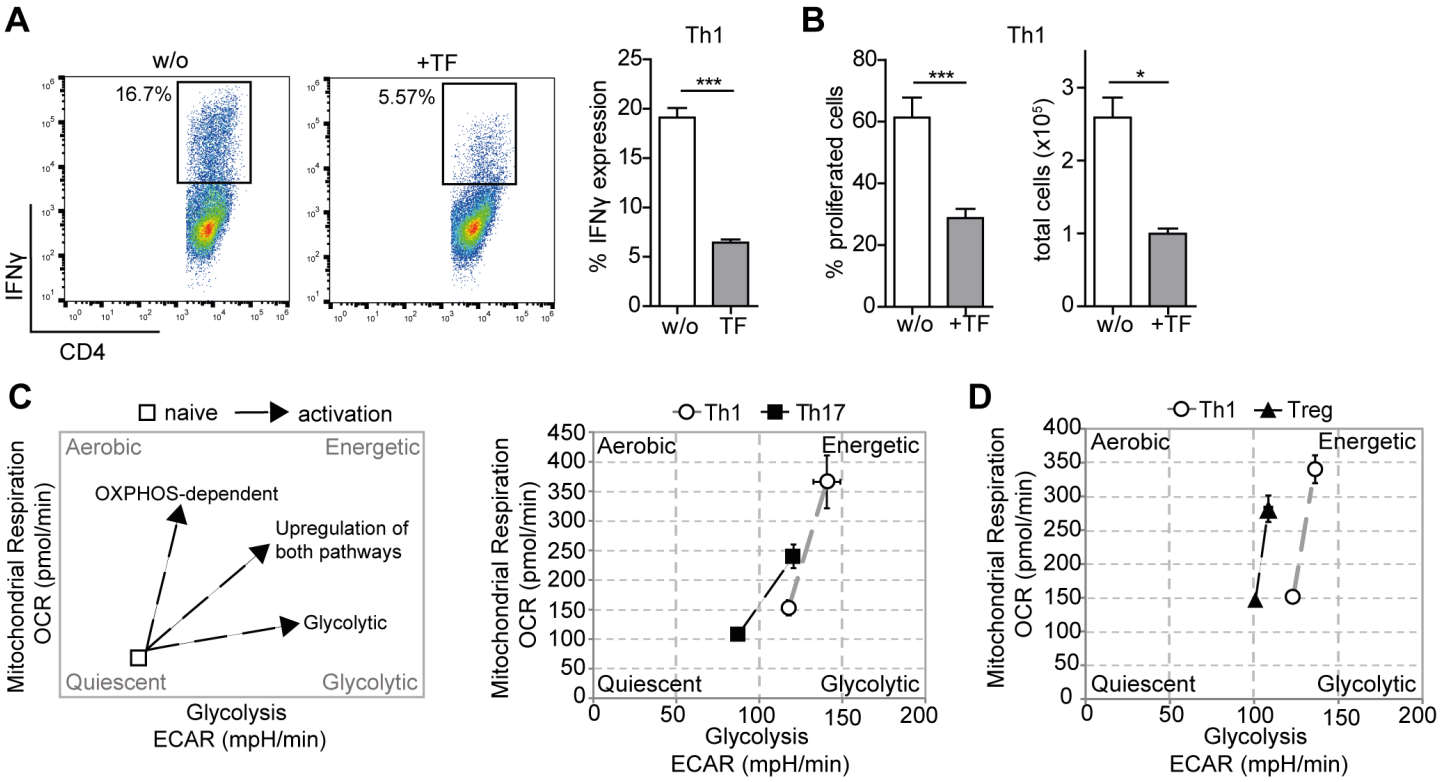

Fig. S7. Effects of teriflunomide on murine Th1 differentiation and proliferation and metabolic capacities of Th1 cells versus Th17 and Treg cells

(A, B) Murine $CD4^+$ T cells were differentiated into Th1 cells for 3 days in presence or absence of teriflunomide (TF). **(A)** IFNγ expression was assessed by flow cytometry via intracellular cytokine staining after restimulation.Data are representative of 3 independent experiments. Bar graph depicts percentages of IFNγ production (n=3). **(B)** Proliferation and absolute cell numbers of Th1-polarized $CD4^+$ T cells in presence or absence of TF at day 6 (n=3). **(C)** XF PhenoGram of *in vitro* Th1- and Th17-polarized murine $CD4^+$ T cells at day 3. Data are representative of 3 independent experiments. **(D)** XF PhenoGram of *in vitro* differentiated murine Th1 and regulatory T cells (Treg) at day 3. Data are representative of 3 independent experiments. All data are displayed as mean ± SEM. Statistical analysis was employed by Student's t-test and was defined as *P≤0.05, **P≤0.01, ***P≤0.001.

Fig. S8

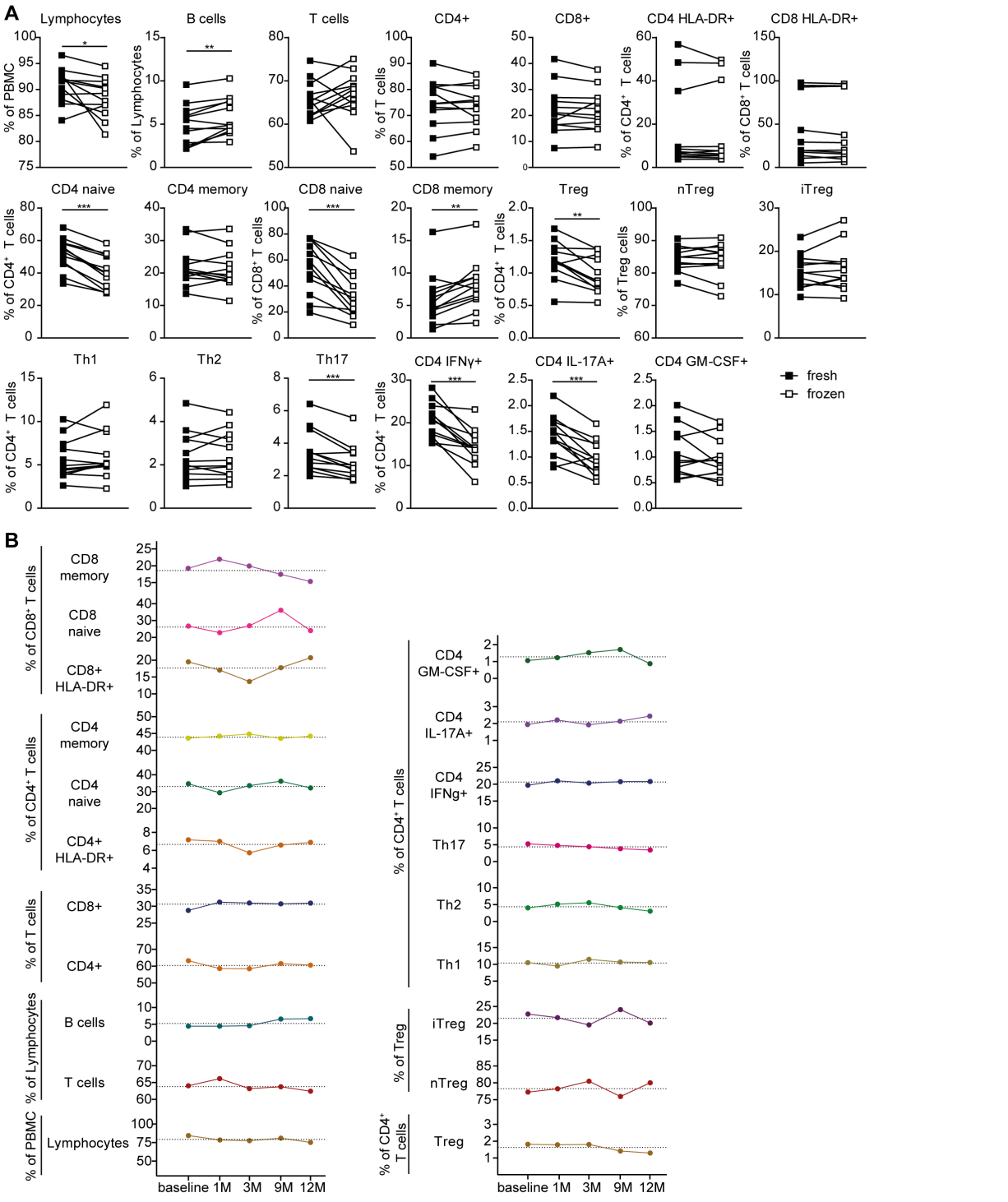
A
Lymphocytes
B cells
T cells
CD4+
CD8+
CD4 HLA-DR+
CD8 HLA-DR+
% of PBMC
% of Lymphocytes
% of T cells
% of CD4+ T cells
% of CD8+ T cells
CD4 naive
CD4 memory
CD8 naive
CD8 memory
Treg
nTreg
iTreg
% of Treg cells
Th1
Th2
Th17
CD4 IFNγ+
CD4 IL-17A+
CD4 GM-CSF+
fresh
frozen
B
CD8 memory
CD8 naive
CD8+ HLA-DR+
CD4 memory
CD4 naive
CD4+ HLA-DR+
CD8+
CD4+
B cells
T cells
Lymphocytes
CD4 GM-CSF+
CD4 IL-17A+
CD4 IFNg+
Th17
Th2
Th1
iTreg
nTreg
Treg
baseline 1M 3M 9M 12M
C
basal respiration
max. respiration
OCR (pmol/min)
D
basal respiration after PMA/Iono stim.
max. respiration after PMA/Iono stim.
E
glycolysis
glycolytic cap.
ECAR (mpH/min)
F
fresh
frozen
glycolysis after PMA/Iono stim.
glycolytic cap. after PMA/Iono stim.

Fig. S8. Comparison of freshly isolated versus frozen PBMC from healthy controls regarding immune cell subset composition and metabolism

(A) Immune cell subset analysis of either freshly isolated or frozen PBMCs from 12 healthy controls (HC) (demographic data depicted in Table S13) by flow cytometry. **(B)** Longitudinal analysis of immune cell subset composition of one HC up to 12 months (12M) by flow cytometry. **(C-F)** $CD4^+$ T cells were either isolated from frozen or freshly isolated PBMCs from the same HCs (n=11) and analyzed for their mitochondrial respiration **(C, D**) or glycolysis **(E, F)** without stimulation or upon short-term stimulation with phorbol 12-myristate 13-acetate (PMA) and Ionomycin for 2.5h (demographic data depicted in Table S14). (OCR: Oxygen Consumption Rate; ECAR: Extracellular Acidification Rate). All data are displayed as mean ± SEM. Statistical analysis was employed by Student's t-test and was defined as *P≤0.05, **P≤0.01, ***P≤0.001.

Fig. S9

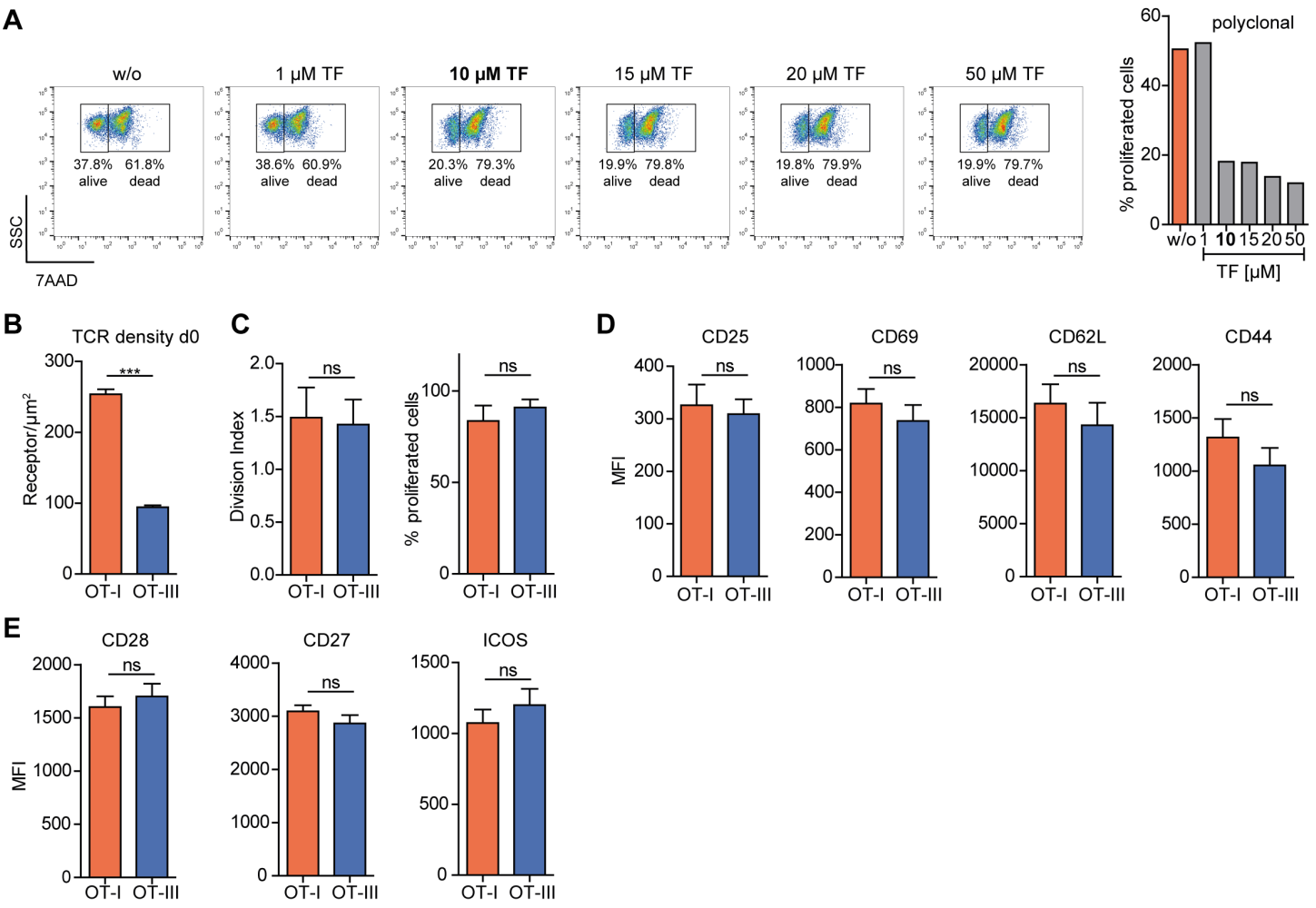

Fig. S9. Additional information supporting methodology

(A) OT-I CD8$^+$ T cells upon stimulation with α-CD3/28 in presence or absence of indicated teriflunomide (TF) concentrations at day 3. Cells were stained with 7-AAD to analyze cell viability and proliferation was assessed by flow cytometry. Dead cells were 7-AAD$^+$. Based on functionality and viability data, 10µM TF was taken for further experiments. **(B)** TCR densities of freshly isolated CD8$^+$ T cells from OT-I (high-affinity TCR) and OT-III (low-affinity TCR) mice at day 0 (n=3). **(C)** Division index and percentages of proliferated OT-I and OT-III CD8$^+$ T cells upon stimulation with $OVA_{257-264}$ peptide in presence or absence of TF at day 3 (n=3). **(D)** Expression of activation markers CD25, CD69, CD62L and CD44 on freshly isolated CD8$^+$ T cells from OT-I and OT-III mice at day 0 (n=3). **(E)** Mean Fluorescence Intensity (MFI) of costimulatory molecules (CD28, CD27 and ICOS) on freshly isolated CD8$^+$ T cells from OT-I and OT-III mice at day 0 (n=3). All data are displayed as mean ± SEM. Statistical analysis was employed by Student's t-test and was defined as *P≤0.05, **P≤0.01, ***P≤0.001.

Table S1. Demographics for all participants and baseline disease characteristics for people with RRMS in the TERIDYNAMIC trial		
Subject Demographics	**Healthy Controls (n=20)**	**RRMS patients (n=50)**
Mean age, years (SD)	42.2 (8.0)	40.7 (9.4)
Female, n (%)	14 (70)	35 (70)
Time since first symptoms of MS, median (min; max), years	N/A	6.67 (0.3;37.0)
EDSS score at baseline, median (min;max)		1.50 (0.0; 4.0)
Naïve to DMT or no DMT >2 years, n (%) **Recently on DMT, n (%)[a]**		16 (32.0) 34 (68.0)
Safety population [a] IFNβ-1 or GLAT, with interruption of ≤3 months and a period of ≥2 weeks without IFNβ-1 or GLAT DMT, disease-modifying treatment; EDSS, expanded disability status scale; GLAT, glatiramer acetate; IFN, interferon; MS, multiple sclerosis; N/A, not applicable; RRMS, relapsing-remitting MS; SD, standard deviation.		

Table S1. Demographics and Baseline Disease Characteristics TERIDYNAMIC trial

Table S2. Differentially regulated genes depicted in Fig.5 I	
Group	**Regulated genes**
OT-I stimulation-dependent genes (unstim vs. stim) 76 genes	Aco2, Agl, Atp5a1, Atp5c1, Atp5d, Atp5o, Atp6v1c2, Cox5b, Cox6a1, Cox6b, Cox7a2l, Cox8a, Cyc1, Eno3, Fbp1, G6pc, G6pdx, Galm, Gsk3b, Idh3g, Mdh1, Ndufa3, Ndufa7, Ndufa8, Ndufb10, Ndufb7, Ndufs1, Ndufs3, Ndufs6, Ndufs7, Ndufs8, Ndufv1, Ndufv2, Oxa1l, Pdhb, Pdk1,Pdk4, Pdpr, Pgam2, Pgk2, Phka1,Ppa1, Ppa2, Prps1l1, Pygl, Rpia, Sdhb, Sdhd, Suclg1, Suclg2, Taldo1, Tkt, Tpi1, Uqcr11, Uqcrc1, Uqcrc2, Uqcrh, Uqcrq, Atp4a, Atp4b, Atp5h, Cox1l, Cox4i2, Eno1, Gapdhs, Gck, Idh1, Idh3b, Lhpp, Ndufab1, Pck1, Pdk2, Pdk3, Pgk1, Pygm, Rbks
OT-III stimulation-dependent genes (unstim vs. stim) 0 genes	-
Affinity-dependent genes (OT-I vs. OT-III) 5 genes	Cox6a2, Cox7a2, H6pd, Ndufv3, Phkb
Affinity-dependent and stimulation-dependent genes 48 genes	Aco1, Aldob, Atp5b, Atp5f1, Atp5g1, Atp5g2, Atp5g3, Atp5j, Atp5j2, Bcs1l, Cox4i1, Cox5a, Cox6c, Cox7b, Dlat, Dld, Dlst, Eno2, Hk3, Mdh1b, Ndufa1, Ndufa10, Ndufa11, Ndufa2, Ndufa4, Ndufa5, Ndufb2, Ndufb3, Ndufb4, Ndufb5, Ndufb6, Ndufb8, Ndufb9, Ndufc1, Ndufc2, Ndufs5, Ogdh, Pgm3, Sdha, Sucla2, Ugp2, Uqcrfs1

Table S2. Differentially regulated genes depicted in Fig.5 I

Table S3. Demographics and Baseline Disease Characteristics of healthy controls and treatment-naïve RRMS Patients analyzed for TCR repertoire changes		
Subject Demographics	**HC (n=10)**	**RRMS (n=14)**
Diagnosis	N/A	14 RRMS
Mean age, years (SD)	42.2 (8.0)	42.5 (8.1)
Female, n (%)	7 (70)	10 (71.4)
Time since first symptoms of MS (SD), years	N/A	6.7 (9.8)
EDSS score at baseline, (SD)		1.5 (1.7)
Naïve to DMT (%)		100
DMT, disease-modifying treatment; EDSS, expanded disability status scale; HC, healthy controls; MS, multiple sclerosis; N/A, not applicable; RRMS, relapsing-remitting MS; SD, standard deviation.		

Table S3. Demographics and Baseline Disease Characteristics of healthy controls and treatment-naïve RRMS Patients analyzed for TCR repertoire changes

Table S4. Demographics and Baseline Disease Characteristics of treatment-naïve RRMS Patients before and during teriflunomide treatment analyzed for TCR repertoire changes	
Subject Demographics	**RRMS (n=20)**
Diagnosis	20 RRMS
Mean age, years (SD)	45.1 (7.9)
Female, n (%)	14 (70)
Time since first symptoms of MS (SD), years	5.9 (5.2)
EDSS score at baseline, (SD)	1.75 (1.5)
Naïve to DMT (%)	100
DMT, disease-modifying treatment; EDSS, expanded disability status scale;MS, multiple sclerosis; RRMS, relapsing-remitting MS; SD, standard deviation.	

Table S4. Demographics and Baseline Disease Characteristics of treatment-naïve RRMS Patients before and during teriflunomide treatment analyzed for TCR repertoire changes

Table S5. Demographics and Baseline Disease Characteristics of treatment-naïve RRMS Patients before and during teriflunomide treatment analyzed for immune cell phenotyping	
Subject Demographics	**RRMS (n=9)**
Diagnosis	9 RRMS
Mean age, years (SD)	47.7 (6.8)
Female, n (%)	6 (66.6)
Time since first symptoms of MS (SD), years	7.1 (5.3)
EDSS score at baseline, (SD)	2.0 (0.6)
Naïve to DMT (%)	100
DMT, disease-modifying treatment; EDSS, expanded disability status scale; MS, multiple sclerosis; RRMS, relapsing-remitting MS; SD, standard deviation.	

Table S5. Demographics and Baseline Disease Characteristics of treatment-naïve RRMS Patients before and during teriflunomide treatment analyzed for immune cell phenotyping

Table S6. Demographics and Baseline Disease Characteristics of RRMS Patients before and during teriflunomide treatment for at least 6 months analyzed for suppressive capacity of Tregs	
Subject Demographics	**RRMS (n=10)**
Diagnosis	9 RRMS/1 CIS
Mean age, years (SD)	42.5 (7.9)
Female, n (%)	7 (70)
Time since first symptoms of MS (SD), years	10.3 (9.0)
EDSS score at baseline, (SD)	2.9 (2.0)
Naïve to DMT, n (%) **Recently on DMT, n (%)**	4 (40) 6 (60)
DMT, disease-modifying treatment; EDSS, expanded disability status scale;MS, multiple sclerosis; RRMS, relapsing-remitting MS; SD, standard deviation.	

Table S6. Demographics and Baseline Disease Characteristics of RRMS Patients before and during teriflunomide treatment for at least 6 months analyzed for suppressive capacity of Tregs

Table S7. Demographics and Baseline Disease Characteristics of RRMS Patients before and during teriflunomide treatment for at least 6 months analyzed for cytokine expression of Tregs	
Subject Demographics	**RRMS (n=18)**
Diagnosis	17 RRMS/1 CIS
Mean age, years (SD)	45.9 (8.6)
Female, n (%)	13 (72)
Time since first symptoms of MS (SD), years	8.1 (5.9)
EDSS score at baseline, (SD)	2.3 (1.6)
Naïve to DMT, n (%) **Recently on DMT, n (%)**	4 (22) 14 (78)
DMT, disease-modifying treatment; EDSS, expanded disability status scale; MS, multiple sclerosis; RRMS, relapsing-remitting MS; SD, standard deviation.	

Table S7. Demographics and Baseline Disease Characteristics of RRMS Patients before and during teriflunomide treatment for at least 6 months analyzed for cytokine expression of Tregs

Table S8. Demographics and Baseline Disease Characteristics of treatment-naïve RRMS Patients before and during teriflunomide treatment for at least 6 months analyzed for myelin specific T cell frequencies	
Subject Demographics	**RRMS (n=3)**
Diagnosis	3 RRMS
Mean age, years (SD)	38.3 (7.93)
Female, n (%)	2 (66.6)
Time since first symptoms of MS (SD), years	3.7 (0.5)
EDSS score at baseline, (SD)	1.5 (1.5)
Naïve to DMT (%)	100
DMT, disease-modifying treatment; EDSS, expanded disability status scale; MS, multiple sclerosis; RRMS, relapsing-remitting MS; SD, standard deviation.	

Table S8. Demographics and Baseline Disease Characteristics of treatment-naïve RRMS Patients before and during teriflunomide treatment for at least 6 months analyzed for myelin specific T cell frequencies

Table S9. Demographics and Baseline Disease Characteristics of treatment-naïve RRMS Patients before and during teriflunomide treatment for at least 6 months analyzed for metabolic activity	
Subject Demographics	**RRMS (n=14)**
Diagnosis	13 RRMS/1 CIS
Mean age, years (SD)	44.5 (7.6)
Female, n (%)	6 (43)
Time since first symptoms of MS (SD), years	5.3 (5.3)
EDSS score at baseline, (SD)	1.8 (0.9)
Naïve to DMT (%)	100
DMT, disease-modifying treatment; EDSS, expanded disability status scale; MS, multiple sclerosis; RRMS, relapsing-remitting MS; SD, standard deviation.	

Table S9. Demographics and Baseline Disease Characteristics of treatment-naïve RRMS Patients before and during teriflunomide treatment for at least 6 months analyzed for metabolic activity

Table S10. Demographics and Baseline Disease Characteristics of treatment-naïve RRMS Patients before and during treatment with Dimethyl fumarate (DMF), interferon-β (IFNβ) and glatiramer acetate (GLAT) analyzed for TCR repertoire changes			
Subject Demographics	**DMF (n=14)**	**IFNβ (n=10)**	**GLAT (n=10)**
Diagnosis	10 RRMS/4 CIS	6 RRMS/4 CIS	6 RRMS/4 CIS
Mean age, years (SD)	40.1 (8.1)	31.5 (6.9)	35.9 (11.7)
Female, n (%)	7 (50)	7 (70)	7 (70)
Time since first symptoms of MS (SD), years	5.3 (5.2)	1.1 (0.4)	0.6 (0.8)
EDSS score at baseline, (SD)	2.0 (1.1)	0.5 (0.7)	1.7 (0.9)
Naïve to DMT (%)	100	100	100
DMF, dimethyl fumarate; IFNβ, interferonβ; GLAT, glatiramer acetate; DMT, disease-modifying treatment; EDSS, expanded disability status scale; HC, healthy controls; MS, multiple sclerosis; RRMS, relapsing-remitting MS; SD, standard deviation.			

Table S10. Demographics and Baseline Disease Characteristics of treatment-naïve RRMS Patients before and during treatment with Dimethyl fumarate (DMF), interferon-β (IFNβ) and glatiramer acetate (GLAT) analyzed for TCR repertoire changes

Table S11. Demographics and Baseline Disease Characteristics of healthy controls and treatment-naïve RRMS Patients analyzed for metabolic activity			
Subject Demographics	**HCs (n=24)**	**RRMS (n=25)**	**RRMS relapse (n=24)**
Diagnosis	N/A	16 RRMS/9 CIS	20 RRMS/4 CIS
Mean age, years (SD)	34.9 (11.5)	34.7 (11.3)	35.4 (12.4)
Female, n (%)	15 (63)	22 (88)	18 (75)
Time since first symptoms of MS (SD), years	N/A	2.2 (3.3)	1.7 (3.1)
EDSS score, (SD)		1.2 (0.8)	1.5 (0.8)
Naïve to DMT (%)		100	100
Definitions: Stable disease was defined as absence of novel clinical symptoms and no MRI activity within at least 4 weeks prior to PBMC collection. Relapse was defined according to acknowledged clinical criteria, e.g. new or deteriorating of neurological symptoms which last for at least 24h in the absence of infection. DMT, disease-modifying treatment; EDSS, expanded disability status scale; HC, healthy controls; MS, multiple sclerosis; N/A, not applicable; RRMS, relapsing-remitting MS; SD, standard deviation.			

Table S11. Demographics and Baseline Disease Characteristics of healthy controls and treatment-naïve RRMS Patients analyzed for metabolic activity

Table S12. Demographics and Baseline Disease Characteristics of HCs and RRMS Patients analyzed for metabolic activity after 72h of *in vitro* stimulation		
Subject Demographics	**HC (n=10)**	**RRMS (n=10)**
Diagnosis	N/A	8 RRMS/2 CIS
Mean age, years (SD)	31.0 (5.0)	32.1 (5.2)
Female, n (%)	7 (70)	7 (70)
Time since first symptoms of MS, median (min; max), years	N/A	8.7 (8.7)
EDSS score at baseline, (SD)		1.8 (1.1)
GLAT, n (%) **IFNβ, n (%)** **NAT, n (%)**		3 (30) 6 (60) 1 (10)
GLAT, glatiramer acetate; IFNβ, interferonβ; NAT, natalizumab; DMT, disease-modifying treatment; EDSS, expanded disability status scale; HC, healthy controls; MS, multiple sclerosis; RRMS, relapsing-remitting MS; SD, standard deviation.		

Table S12. Demographics and Baseline Disease Characteristics of HCs and RRMS Patients analyzed for metabolic activity after 72h of in vitro stimulation

Table S13. Demographics and Baseline Disease Characteristics of healthy controls analyzed for immune cell phenotyping of freshly isolated versus frozen PBMCs	
Subject Demographics	**HC (n=12)**
Mean age, years (SD)	30.3 (4.0)
Female, n (%)	9 (67)
HC, healthy controls; SD, standard deviation	

Table S13. Demographics and Baseline Disease Characteristics of healthy controls analyzed for immune cell phenotyping of freshly isolated versus frozen PBMCs

Table S14. Demographics and Baseline Disease Characteristics of healthy controls analyzed for metabolic differences of T cells isolated from fresh blood or frozen PBMCs	
Subject Demographics	**HC (n=11)**
Mean age, years (SD)	31.2 (5.1)
Female, n (%)	6 (55)
HC, healthy controls; SD, standard deviation	

Table S14. Demographics and Baseline Disease Characteristics of healthy controls analyzed for metabolic differences of T cells isolated from fresh blood or frozen PBMCs